Electronic Supplementary Material (ESI) for Chemical Communications

Supporting Information

Probing the Metal Specificity Mechanism of Superoxide Dismutase from human pathogen *Clostridium difficile*

Wei Li[a]†, Hongfei Wang[b]†, Zheng Chen[a], Qing Ye[c], Yang Tian[c], Xin Xu[a], Zhongxian Huang[a], Pingwei Li[d], and Xiangshi Tan[a]*

[a]Department of Chemistry & Institutes of Biomedical Sciences, Fudan University, Shanghai 200433, China.

[b]Institute of Opto-Electronics & Institute of Molecular Science, Shanxi University, Taiyuan 030006, China

[c]Department of Chemistry, Tongji University, Shanghai, China

[d]Department of Biochemistry and Biophysics, Texas A & M University, TX77843, USA

*To whom correspondence should be addressed. Email: xstan@fudan.edu.cn

Preparation of SOD$_{cd}$ enzymes

The superoxide dismutase from human pathogen *C. difficile* (SOD$_{cd}$) was prepared similarly as described[1]. The SOD$_{cd}$ gene was amplified from *C. difficile* genomic DNA as a template using a pair of primers:

5'-TA**GGATCC**CCTGAAAATAACAAATTTAAGG-3'(F);

5'-CC**CTCGAG**TTAATCTTGAGATTTTAAATTTTTG-3'(R).

The PCR products digested *by BamH* I and *Xho* I (*New England Biolabs*) were ligated into the linearized MBPHT-mCherry2 vector with an N-terminal maltose binding protein followed by 8× histidine tag and TEV protease cleavage site. The resulting ligation mixture was transformed into XL10-Gold competent cells (*Novagen*) by heat shock. The recombination plasmid was verified by DNA sequencing (*Invitrogen*) and transformed into Rosseta (DE3) pLysS competent cells (*Novagen*), which grew in modified LB media containing 50μg/ml ampicillin and 34 μg/ml chloramphenicol with vigorous shaking at 37 ℃ until an OD_{600} of 0.6 was attained. The expression was induced with the addition of 0.3 mM isopropyl-1-thio-D-galactopyranoside (IPTG) and further incubated at 37 ℃ for 8 hours. Cells were collected by centrifugation at 4500×g for 10 min at 4 ℃ using a Sorvall (RC-6C Plus) centrifuge. Cell pellets were re-suspended in 20 mM potassium phosphate, pH 7.4, 25 mM imidazole, 500 mMNaCl, 1 mM PMSF. Then the cells were sonicated and centrifuged at 12,000×g for 30 min to clarify the lysate. The lysate was purified by a preformed Ni-NTA His-Trap gravity column (*Qiagen, Chatsworth, CA*). SOD$_{cd}$ fractions were then tested for initial purity by SDS-PAGE and subjected to TEV protease for incision. After cleavage of the N-terminal maltose binding protein (MBP) tag, the protein solution was subjected to Ni–NTA column again to remove the MBP tag. Pure (>85%) fractions were combined, and subjected to the ÄKTA *purifier* FPLC system and passed over a HiLoad™ 16/60 Superdex™ 200 gel filtration column. Fractions were analyzed by SDS-PAGE (which indicated >95% purity), combined, and concentrated for storage at -80 ℃. Protein concentrations of SOD samples were determined by the Bradford Method similarly as described.

To obtain metal (Mn, Fe, and Co) ion solely occupied SOD_{cd}, The method of denaturing and refolding method was used with denaturant (urea) and chelator (8-hydroxyl quinoline) according to literature[2]. The purified (Milli Q) water for this experiment was treated by Chelex-100 resin (Bio-Rad). The isolated SOD_{cd} protein (~20 mg) was treated with 20 mM TrisHCl (pH 3.4) containing 8 M urea, 10 mM 8-hydroxyl quilionine and 2 mM dithiothreitol (DTT) for 30 min. The Apo-SOD_{cd} was obtained by dialyzing against 40 mM TrisHCl (pH 7.8), 8 M urea, 2 mM 8-hydroxyl quilionine and 1 mM DTT for 5 h, then against 20 mM TrisHCl, pH 7.8, containing 1 mM 8-hydroxyl quilionine and 1 mM DTT overnight, and finally against 20 mM TrisHCl, pH 7.8, for 12 h. The Fe-sub-$MnSOD_{cd}$, $MnSOD_{cd}$, and Co-sub-$MnSOD_{cd}$ were prepared by dialyzing of the apo-enzyme in 10 mM TrisHCI, pH 7.8, 8 M urea and 2 mM DTT containing 2 mM $FeSO_4 \cdot 7H_2O$, 1 mM $MnCl_2$ and 1 mM $CoCl_2 \cdot 7H_2O$ for 2h, respectively.

To examine the metal selectivity for SOD_{cd}, the unfolding Apo-SOD_{cd} was treated with the metal mixture including Mn^{2+}, Fe^{2+}, Co^{2+}, Ni^{2+}, Cu^{2+}, Zn^{2+} (0.5 mM). Urea was removed by dialyzing the solution against 20 mM TrisHCl, pH 7.8, containing 0.2 mM metal salts and 1 mM DTT overnight, then against 20 mM TrisHC1, pH 7.8, 0.1 mM DTT for 6 h for three times. The precipitate formed during dialysis was removed by centrifugation. The clear SOD_{cd} protein solution was applied to a Source 15S column equilibrated with 10 mM potassium phosphate at pH 7.8. The SOD_{cd} enzyme was eluted from the column with 50 mM potassium phosphate, pH 7.8. The SOD_{cd} protein concentration was determined by Bradford method[3]. The enzymes with sole metal bound were subjucted to ICP/MS analysis.

Metal Analysis of different metal substituted SOD_{cd}

The metal determination and quantification were performed according to Hall *et al.* with minor modifications[4]. Briefly, ICP/MS was operated on an Elan DRC II ICP-MS from Perkin-Elmer. An analog detection mode was used with three averaged replicates per reading. External calibration standards were prepared through the serial dilution of a single 10 ppm stock mixture of Mn, Fe, Co and Ni ions in 2% trace select nitric acid from Fluka. Freshly prepared standards generally contained 2, 20, and 200 ppb of the metal ions in 1% nitric acid, diluted in MilliQ deionized water. The metal content of proteins was determined by overnight digestion in 1M HNO_3 (Trace Metal Grade). Digested samples were diluted to 0.2 M HNO_3 for analysis. The results were listed in **Table S1**.

Spectroscopy:

Fluorescence spectra were recorded using a Cary Eclipse Spectrofluorimeter (Varian)[5]. The metal uptake studies were initiated by adding an aliquot of the metals stock solution ($MnCl_2$, $CoCl_2$, $NiCl_2$ and Ferric citrate) to a thermally equilibrated, stirred solution of 50 µg/ml Apo-SOD_{cd} buffered in 20 mM HEPES, pH 7.2, 100 mM NaCl. Emission intensity was monitored at 333 nm using a dynode voltage of 680 V with 1 s^{-1} sampling frequency. The kinetic time courses were imported into Origin 8.0 and fitted by a multi-exponential decay process **(Fig. S2)**.

The far-UV CD[6] (200 nm-250 nm) spectra of these SOD_{cd} were recorded on a Jasco 720 Spectrometer using a 2.0 mm quartz cuvette. The data were recorded every 0.2 nm at a rate of 100 nm/min. The samples containing 10 µM Apo-SOD_{cd}, 20 mM HEPES, pH 7.2, 100 mM NaCl in presence of desired metals (0.1 mM) were heated from 30 ℃-90 ℃ at a rate of 2 ℃/min, and ellipticity was monitored at 222 nm; the melting temperature[7] were determined as reported previously[8]. T_m value was calculated according to eq.1 and solved for T at which $\Delta G = 0$: $\Delta G = -RT\ln[(I_F - I) / (I - I_U)]$ (1), Where I is the ellipticity at 222 nm at temperature T, I_F is the initial (folded) ellipticity, and I_U is the final (unfolded) ellipticity. The intensity was normalized by eq.2 : fraction changes of ellipticity = $(I_F - I) / (I_F - I_U)$ (2). The results were presented in **Fig. S3**.

Electronic absorption spectra of SOD_{cd} enzymes were recorded on a HP8453 UV–visible spectrophotometer **(Fig. S4)**. The metal valence determination was performed by titration with reductant dithionite and oxidatant $KMnO_4$. As shown in

Fig. S5, the isolated $MnSOD_{cd}$ is mainly in +3 states, partly with the +2 covalence mixure while Fe-sub-$MnSOD_{cd}$ is in +3 state solely in isolated sample[9].

4K EPR spectra were recorded on a Bruker EMX X-band spectrometer equipped with an Oxford-910 cryostat and ITC-503 temperature controller (Oxford Instruments Ltd.) **(Fig. 1)**. All SOD_{cd} samples (~15 mg/ml) were frozen in the presence of 10% glycerol. Experimental conditions: temperature 4K, microwave frequency 9.44 GHz, power 2.0 mW, modulation at 100 kHz, modulation amplitude 4 G, and time constant, 163.84 ms.

SOD Activity assay

The catalytic activity of SOD_{cd} was measured by the method described by McCord and Fridovich[10], using inhibition of the xanthine/xanthine oxidase[11]-induced reduction of cyt *c* **(Fig. S6)**. A 3.00 ml reaction system includes the following ingredients: 2.8 ml of 50 mM potassium phosphate, 0.1mM ethylenediaminetetraacetic acid, 0.01 mM cytochrome *c*, 0.05 mM xanthine, 0.1 ml XO and 0.1 ml SODs or distilled water. The SOD activity was calculated as following:

$$\%\ \text{Inhibition} = \frac{\Delta A_{550nm}\ /\text{min Uninhibited} - \Delta A_{550nm}\ /\text{min Inhibited}}{\Delta A_{550nm}\ /\text{min Uninhibited} - \Delta A_{550nm}\ /\text{min Blank}} \times 100$$

$$\text{Units/ml enzyme} = \frac{\%\ \text{Inhibition} * (\text{df})}{(50\%) * (0.1)}$$

Where, df = Dilution factor; 0.1 = Volume (in milliliter) of enzyme used; 50% = Inhibition of the rate of cytochrome c reduction as per the unit definition).

Stopped-flow spectroscopy

To obtain the second reaction rate and the K_m or k_{cat} values for SOD_{cd}, the stopped-flow kinetics were performed using KO_2 as the superoxide source[12] **(Fig. S7)**. KO_2 (Sigma-Aldrich) with an equal-molar amount of 18-crown-6 ether were dissolved in dry DMSO. A double mixing stopped-flow spectrophotometer (TgK Scientific Limited, SF-61DX2) was applied to monitor the absorption change of superoxide at 260 nm (ε_{250} =2000 M^{-1} cm^{-1}). Substrate concentration change was achieved by altering the initial KO_2 concentration. The initial $O_2^{\cdot-}$ concentration was calculated by the molar extinction coefficient at 260 nm. The experimental process was as following: firstly, KO_2 in DMSO in a 250μL syringe was mixed in a 1:10 ratio with an aqueous solution at pH 11 containing 2 mM CAPS (sigma) and 1 mM EDTA. After a 500 ms delay, the KO_2 solution was rapidly mixed in a 1:1 ratio with 100nM SOD_{cd} in 100 mM potassium phosphate with 1 mM EDTA at pH 9.5. The mean of three or four catalytic traces was recorded and fitted with the first exponential decay as pseudo-first order reaction for $O_2^{\cdot-}$ in Origin 8.0. The second reaction rate was obtained using the pseudo first order rate dividing the SOD concentration. Due to the instability of $O_2^{\cdot-}$ in the low pH buffer, the values obtained by this method were under pH 9.5. All the final SOD rates were obtained by subtracting the $O_2^{\cdot-}$ auto-disproportionation rate (at pH 9.5, k = ~2000 $M^{-1}s^{-1}$)[13]. All the SOD_{cd} activity results were summarized in **Table S1**.

Crystallography

$MnSOD_{cd}$, Fe-sub-$MnSOD_{cd}$ and Co-sub-$MnSOD_{cd}$ (~20 mg/ml) were crystallized by hanging-drop vapor diffusion method at 16°C under in 60% v/v tacsimate^{TM} at pH 7.0. The SOD_{cd} crystals were frozen in the cryostream and the diffraction data were collected using beamline BLXU17 of Shanghai Synchrotron Facility (SSRF) using an ADSC QUANTUM 315 detector with wavelength of 0.9792 Å. The diffraction data were processed and scaled with HKL-2000[14]. The structures were solved by molecular replacement by MOLREP[15] using the 1.6 Å structure of *B. subtilis* Superoxide Dismutase (PDB code 2RCV)[16] as the starting model. All water molecules and metal atoms were omitted from the starting model. The best solution yielded one monomer in the asymmetric unit. After simulated annealing refinement, the R_{cryst} was 32.3% (R_{free} = ~33.5%) for data between 25 and 2.5 Å resolution. Subsequent cycles of model building, isotropic B-value, and positional refinement to 1.8-2.2 Å resolution were performed using REFMAC5[17], COOT[18] and PHENIX[19]. At this point, the metal ions and their ligands were modeled into the active sites, and the orientations of the side chains of polar amino acids, dual conformers, and bound water molecules were modeled according to F_o-F_c Fourier maps countered at 3σ level. Occupancies of dual conformers were manually adjusted until positive and negative F_o-F_c density peaks were disappeared. After all the models were build, the positions of the coordination residues was carefully fitted with Real Space Refine Zone in PHENIX to make sure that the residues matched density well and were in the center of density. In the last stages of refinement, anisotropic B factors were refined. Finally, water molecules were added using PHENIX and positioned only if well defined positive peaks were present in both the $2F_o$-F_c and F_o-F_c electron density maps, and/or if they were within hydrogen-bonding distance with either protein atoms or other presumed water molecules. Modeled water molecules that refined with B factors above three times the average protein B-value were deleted. The final structures were refined to R_{cryst} = 16.3% and R_{free} = 18.8% for $MnSOD_{cd}$, R_{cryst} = 18.0% and R_{free} = 20.3% for Fe-sub-$MnSOD_{cd}$, R_{cryst} =18.2% and R_{free} = 19.0% for Co-sub-$MnSOD_{cd}$, respectively. The quality of the models were checked using PROCHECK[20]. The data collection and refinement statistics were listed in **Table S2**. Structural figures were prepared using PyMOL[21] **(Fig. 2 and Fig. S8)**. All the structures of SOD_{cd} have been deposited in the Protein Data Bank (PDB), with the accession codes of 4JZG ($MnSOD_{cd}$), 3TJT (Fe-sub-$MnSOD_{cd}$) and 4JZZ (Co-sub-$MnSOD_{cd}$), respectively.

Fe K-edge X-ray absorption and X-ray fluorescence spectrum of Fe-sub-$MnSOD_{cd}$

The metal fidelity of Fe-sub-$MnSOD_{cd}$ crystal was confirmed by X-ray absorption and X-ray fluorescence spectrum **(Fig. S9).** Standard excitation and MAD scans operations were done[22]. Briefly, the rhombic crystal of Fe-sub-$MnSOD_{cd}$ was flash-cooled and mounted under a liquid N_2 stream. Then the BLU-ICE softerware was used to selective the excitation scan energy for Fe element from the periodic table (500.0 eV above the edge energy). The wavelength changes were conducted automatically and X-ray beam intensity was optimised at each stage. The scan time was increased to improve the signals. Then the incident 1.74 Å X-ray (BL17U1, in

Shanghai synchrotron radiation faculty, SSRF) was focused on the crystal and the absorption spectrum was collected. After collecting, BLU-ICE will automatically search for peaks and attempted to match them to the emission energy for all the stable elements. The peak dispalyed in our exitation spectrum corresponded to Fe element only, indicating the metal purity of this sample. Further, X-ray fluorescence [9] scans were performed using excitation of the Fe K-edge energy. The Fe-K edge EXAFS signals confirmed metal fidelity of Fe-sub-MnSOD$_{cd}$.

Electrochemistry

(1) *Potentiometric Titration*

Potentiometric titrations were performed using a Ag/AgCl/Pt electrode at 25 ℃ with an optical cell according to Stankovich method[23] **(Fig. S10 and Fig. 3)**. A combination of Ag/AgCl/Pt electrode was inserted in one port, a syringe containing titrant was mounted in a second, and the third port was connected to a vacuum line and maintained a low flow of N_2 gas to remove residual O_2. The reaction buffer contained 50 mM potassium phosphate at pH 7.8, containing 100 mM NaCl, 0.4 mM SOD$_{cd}$. The mediators were 25μM p-benzoquinone for MnSOD$_{cd}$, and 10μM DCIP for Fe-sub-MnSOD$_{cd}$, respectively. Fe-sub-MnSOD$_{cd}$ was reduced by dithionite, and the reduced form then was oxidized by titration of aliquots of $KMnO_4$. The absorbance of Fe-sub-MnSOD$_{cd}$ at 350 nm and electrochemical potentials were monitored during the oxidation titration process. For the MnSOD$_{cd}$, the sample in each equilibrating potential point was withdrawn, frozen in the liquid N_2 quickly for EPR spectra collection. For the determination of reduction potentials, the deduced percentage of the oxidation SOD species was plotted as a function of the reduction potential at equilibrium. The data were fit with the Nernst equation: $E = E_m + 0.059 \log(Ox/(100-Ox))$, where E is the measured ambient potential in Voltage, Ox is the percentage of oxidized SOD and E_m is the reduction midpoint potential. Although the mediators and the potentials responded rapidly to titrant additions, they equilibrated slowly with SODs, reaching equilibrium after up to 4 h, as reported by other groups[24]. During this long equilibrium process, SOD_{cd} lost some metals and its activity was compromised. Hence, we failed to perform the back titrations and the Nernst reversibility cannot to be obtained from our titrations. Considering to drawbacks of the titration experiments, We further performed the CV scans to get the reduction midpoint potentials of SODs **(see below)**.

(2) ***Cyclic Voltammetry***

Cyclic voltammetry (CV) of immobilized SOD_{cd} was carried out with BAS 100B/W electrochemical analyzer [25] and the CHI 604A (Shanghai Chenhua instrument, China) **(Fig. S11)**. A 5 ml compartment with a three-electrode configurations was used as the electrochemical cell. A platinum wire was the counter electrode. The reference electrode was an Ag/AgCl, 1M KCl electrode. The SOD_{cd} immobilized glassy carbon electrode was used as working electrodes. The SOD_{cd} immobilized glassy carbon electrode modification process was performed in the ambient aerobic air as following: the naked glassy carbon electrode was boiled in 2.5

M KOH for 4 h, sonicated for 5 min, then rinsed with Millipore water and stored in concentrated sulfuric acid (H_2SO_4, 95～97%) overnight. Before modification, the electrodes were rinsed with water, treated with concentrated nitric acid (HNO_3, 65%) for 10 min and rinsed again with Millipore water. The bare GC electrode was further activated by CV scan in 0.5M H_2SO_4 electrolyte between -1.0 V and 1.0 V at 0.2 V/S^{-1}. For SOD_{cd} adsorption, the cleaned electrodes were first incubated in 2 mM Ni-NTA aqueous solution (formed by mixing Ni^{2+} solution and NTA solution at room temperature under constant stirring for overnight) for overnight at low temperature, then incubated in 1 ml 200 μM of SOD_{cd} in 50 mM PBS buffer pH 7.5 at 4 ℃ for 12 h. Further addition of EDC (N′-ethylcarbodiimide hydrochloride) (200 mM stock solution in water) with a final concentration of 5 mM for 30 min was used for covalent immobilization of SOD_{cd}. CV of SOD_{cd} solution was performed between -500 and +500 mV at different potential scan rates in 50 mM PBS buffer pH 7.4. The buffer was always purged with high pure N_2 before use to remove residual O_2. The almost unchanged CV profiles along with long time scans at the rate of 100 mV/s confirmed the stability and reproducibility of our SOD modified electrodes **(Fig. S12)**. To ascertain the activity of the immobilized SOD_{cd}, the amperometric titrations on SOD/NTA modified electrodes using KO_2-DMSO solution were also performed[26] **(Fig. S13)**. To evaluate the mass transport process of these SOD immobilized electrodes, the variation scans at different potential rates were performed **(Fig. S14).**

Optical, EPR titration and azide affinity

Optical pH titrations of $MnSOD_{cd}$ and Fe-sub-$MnSOD_{cd}$ were performed using Hewlett-Packard 8453 spectrophotometer **(Fig. S15)**. pH values were measured continuously using a combination pH microelectrode (Microelectrodes Inc.). pH was increased in a small step by adding 100 mM KOH and then the optical spectrum was recorded at each pH value. pK value was obtained by fitting the data with the Henderson-Hasselbalch equation $(A_A-A_{obs})/(A_A-A_B) = (K)/(K+10^{-(pH)})$, where A_A and A_B (as the acid and base forms) are absorbance values at 476 nm, respectively, A_{obs} is the observed absorbance at a given pH value, K is the acid dissociation constant and the Hill coefficient is set to 1. The EPR pH titration was performed as follows **(Fig. S16)**: The pH values of Fe-sub-$MnSOD_{cd}$ were adjusted successively with 100 mM KOH. The SOD_{cd} sample at each pH point, measured using a microelectrode, was transferred into an EPR tube and promptly frozen in liquid nitrogen. Signal amplitudes in the spectra were plotted as a function of pH values. The *pK* values were evaluated by fitting with the Henderson-Hasselbalch equation neglecting cooperativity.

Azide binding ability with these SOD_{cd} proteins was determined by titration of azide to the different SOD_{cd} proteins, respectively, using Hewlett-Packard8453 spectrophotometer at 25℃ **(Fig. S17)**. The apparent dissociation constant of azide to each SOD_{cd} protein was obtained by fitting the absorbance data to the following eq (1), which describes weak binding with an invariant absorbance background B and addition absorbance A_{max} when SOD protein saturated with azide.

$$A([S])= A_{max}* [S]/(K_d' + [S]) + B \qquad (1)$$

The apparent K_d was corrected for the pK (4.7) of N_3H based on the equilibrium ($N_3H \rightarrow H^+ + N_3^-$) using eq (2), generating the azide dissociation constant K_d'.

$$K_d' = (1+10^{(pH-pK)})K_d \qquad (2)$$

DFT Calculations

(1) DFT Models

From the crystal structures of $MnSOD_{cd}$, Fe-sub-$MnSOD_{cd}$ and Co-sub-$MnSOD_{cd}$, the metal coordination environment and the additional second-sphere residues Tyr64 and Gln178 were extracted. In all cases, the amino-acid residues were truncated at their Cα atoms by replacing the adjacent backbone atoms with H atoms. The terminal methyl of the ligands (including His56, His111, His197 and Asp193), as well as the terminal methyl of Gln178 and Tyr64, were restrained when the geometries optimization were performed **(Table S4 and Fig. S18)**. For the metal ions models, solvent effects also were considered by coordinating the sixth water to each metal ion and using the integral equation formalism polarizable continuum model (IEFPCM)[27, 28].

(2) Computational details

All calculations were carried out with the GAUSSIAN 09 software package. All geometries were fully optimized with the hybrid density functional theory (DFT) at the B3LYP/6-31G (d,p) level, except for iron, cobalt and manganese atoms, which were optimized with the B3LYP/6-31G(2d,p) method[29-31]. The final electronic energies are calculated at the level of B3LYP/ 6-31+G (d,p), except for metal (manganese, iron and cobalt) atoms, which were calculated with the B3LYP/6-31+G(2d,p) method and vibrational frequencies are analytically computed at the same level in order to confirm that a local minimum has no imaginary frequency. Geometries were considered converged when the maximum energy change between subsequent cycles dropped below 10^{-3} hartree and the maximum Cartesian gradient was less than 10^{-2} hartree/Å**.**

(3) The reaction free energy ΔG of metal substitution reactions

To assess the relative metal binding affinities for SOD_{cd}, we designed metal substitution reactions 1 and 2. The reaction free energy (ΔG) was obtained from the calculated G at 298 K and 101 kPa of each reactant and product. Fe^{3+} was chosen because that Fe^{3+} was used in the experimental part.

$$[Fe(H_2O)_6]^{3+}\,(aq) + Mn^{2+}SOD \text{ ----- } Fe^{3+}SOD + [Mn(H_2O)_6]^{2+}\,(aq) \qquad \textbf{(1)}$$

$$[Co(H_2O)_6]^{2+}\,(aq) + Mn^{2+}SOD \text{ ----- } Co^{2+}SOD + [Co(H_2O)_6]^{2+}\,(aq) \qquad \textbf{(2)}$$

The results were listed in **Table S5 and Table S6**. For **equation 1**, When Mn^{2+} was substituted by Fe^{3+}, the reaction energy ΔG at 298 K and 101 kPa is 24.25 kcal/mol, indicating that $Mn^{2+}SOD_{cd}$ was stable than $Fe^{3+}SOD_{cd}$. On the other hand, for **equation 2**, when Co^{2+} substituted Mn^{2+}, the reaction energy ΔG at 298 K and 101 kPa was -17.69 kcal/mol, indicating $Mn^{2+}SOD_{cd}$ was less stable than $Co^{2+}SOD_{cd}$, which was consistent with experiments.

(4) Perturbation Theory Energy Analysis

To investigate the roles of the second coordination key residues in the H-bond network involving in the catalytic process, natural bond orbital analysis was performed. The related atom coordinates at single point energy equilibrium were shown in **Table S4 and Fig. S18**. Perturbation theory energy analysis was carried out by examining all possible interactions between "filled" (donor) Lewis-type NBOs and "empty" (acceptor) non-Lewis NBOs, and estimating their energetic importance by 2nd-order perturbation theory. At large inter-atomic separations, the NAOs $\{\theta_i^{(0)}\}$ essentially reduce to the corresponding atomic natural orbitals[32 33] of isolated atoms. However, in a given molecular environment, the NAOs reflect the chemical give and take of electronic interactions, with variations of shape (e.g., angular deformations due to steric pressures of adjacent atoms) and size (e.g., altered diffuseness due to increased anionic or cationic character) that distinguish them appreciably from free-atom forms. Given an effective one-electron Hamiltonian **F** (e.g., Fock or Kohn–Sham operator) for the system, with associated NAO orbital energies $\varepsilon_i^{(0)}$,

$$\varepsilon_i^{(0)} = \left\langle \theta^{(0)}{}_i \middle| \mathrm{F} \middle| \theta^{(0)^*}{}_i \right\rangle \tag{1}$$

The interaction of unperturbed donor $\varphi_i^{(0)}$ (e.g., a valence lone pair) with acceptor $\varphi_{j*}^{(0)}$ (e.g., a valence anti-bond) leads to the corresponding second-order $i \rightarrow j^*$ stabilization estimate[34],

$$\Delta E_{i \rightarrow j^*}^{(2)} = -2\left\langle \varphi_i^{(0)} \middle| F \middle| \varphi_{j^*}^{(0)} \right\rangle^2 \Big/ \left(\varepsilon_{j^*}^{(0)} - \varepsilon_i^{(0)} \right) \tag{2}$$

The natural bond orbital second order perturbation theory output displayed "E (2)".

The results were listed in **Table S7**, showing that the Gln178 couples more to Tyr64 in $MnSOD_{cd}$ than that of Fe-sub-$MnSOD_{cd}$ [E(2) of Glu178-Tyr64 are

~5.97/5.87 kcal/mol in reduced state and are ~3.10/2.77 kcal/mol in oxidatized state for $MnSOD_{cd}$/Fe-sub-$MnSOD_{cd}$]. On the other hand, Gln178 of $MnSOD_{cd}$ coupled less to the coordination water than that of Fe-sub-$MnSOD_{cd}$ [E(2) are ~0.43/0.74 kcal/mol in reduced state and ~2.62/4.36 kcal/mol in oxidized state for $MnSOD_{cd}$/Fe-sub-$MnSOD_{cd}$]. Here, we could see that in the oxidized Fe-sub-$MnSOD_{cd}$, Gln178 is tighter to the coordination hydroxyl, which may lower its redox potential and thus impact its catalytic activity. The DFT calculation results likely support the structural features regarding to the polarization patterns of the hydrogen bond network and give a reasonable conjecture that the metal reactivity of the SOD_{cd} may be tuned by the subtly differences in the hydrogen bond network.

Table S1. Summary of metal contents, electrochemical E_m values and SOD activity of SOD_{cd} enzymes.

Sample	Specific activity ($U\ mg^{-1}$)[1]	The second reaction rate ($10^8\ M^{-1}S^{-1}$)	K_m[2] (μM)	k_{cat} (S^{-1})	k_{cat}/K_m ($M^{-1}\ S^{-1}$)	Metal Contents (mol/mol per monomer)				Metal oxidation state[4]	Electrochemical E_m values (mV *vs* NHE)
						Mn	Fe	Co	Ni		
$Apo\text{-}SOD_{cd}$	-[3]	-	-	-	-	-	-	-	0.01	-	-
$Mixed\text{-}SOD_{cd}$[5]	-	-	-	-	-	0.24	0.1	0.47	0.02	-	-
$MnSOD_{cd}$	8600 ±40	6 ±0.2	2	3000	6×10^8	0.51	0.02	-	-	+2/+3	480
$Fe\text{-}sub\text{-}MnSOD_{cd}$	800 ±20	0.2 ±0.03	18	360	2×10^7	-	0.72	-	-	+3	120
$Co\text{-}sub\text{-}MnSOD_{cd}$	-	-	-	-	-	-	-	0.82	-	+2	>700

Note: 1. units/mg of protein/mol of metal ions /mol of subunit. 2. From the stopped-flow measurement in this research. 3. "-" Standing for not be detected. 4. As determined in this report by UV/vis spectra (supporting information). 5. This protein was prepared in the presence of various metals containing Mn, Fe, Co, Ni.

Table S2. Summary of data collection and refinement statistics of SOD_{cd} enzymes.

	$MnSOD_{cd}$	Fe-sub-$MnSOD_{cd}$	Co-sub-$MnSOD_{cd}$
Wavelength	0.9795	0.9792	0.9792
Space group	$P6_522$	$P6_522$	$P6_522$
Unit-cell dimensions (Å, °)	a=80.592, b = 80.592, c=249.509 α=β=90, γ=120	a=80.399, b=80.399, c =251.631 α=β=90, γ =120	*a* =80.321, *b* =80.321, *c* =250.991 *α*=*β*= 90, *γ* =120
Resolution (Å)	2.32	1.8	1.95
No. of observations	363844	882131	319042
No. of unique reflections	21721 (1055) [a]	44038 (2261)[a]	35695 (1756)[a]
Completeness (%)	99.9 (100.0)	96.3(100.0)	98.8 (100.0)
<I>/(I)	37.5 (11.7)	22.9 (12.5)	17.8 (3.2)
Redundancy	16.7 (18.0)	20.0(21.4)	8.9 (9.0)
R_{sym} [b]	0.084 (0.370)	0.133 (0.386)	0.144 (0.392)
R_{cryst} [c] (%)/R_{free} [d] (%)	16.3 / 18.8	17.9 / 20.3	18.2 / 19.1
RMSD bonds (Å) / angles (°) [e]	0.007 / 0.967	0.006 / 0.979	0.007 / 0.978
DPI coordination errors (Å)[f]	0.128	0.080	0.084
Ramachandran plot, residues in:			
Most favored regions (%)	91.2	92.3	92.3
Additional allowed regions (%)	7.1	6.6	6.6
Generously allowed regions (%)	1.6	1.1	1.1
Disallowed regions (%)	0.0	0.0	0.0

[a] Numbers in parentheses represent values in the highest resolution shell (Å). [b] $R_{sym} = \Sigma|I_j-\langle I\rangle|/\Sigma I_j$**, where** I_j **is the observed integrated intensity, <I> is the average integrated intensity obtained from multiple measurements, and the summation is over all observed reflections. [c]** $R_{cryst} = \Sigma||F_{obs}|-|F_{calc}||/\Sigma|F_{obs}|$, F_{obs} **and** F_{calc} **are observed and calculated structure factor amplitudes, respectively. [d]** R_{free} **calculated with randomly selected reflections (5%). [e] Based on the ideal geometry values of Engh & Huber (1991). [f] The errors associated with the bond lengths were calculated from the Cruickshank diffraction-component precision index (DPI)[35].**

Table S3. Bond lengths and bond angles at metal active sites and the hydrogen bond networks of SOD_{cd} enzymes.

	$MnSOD_{cd}$	**Fe-sub-Mn SOD_{cd}**	**Co-sub-Mn SOD_{cd}**	**MnSOD *H. sapiens*[2]**	**FeSOD *E.coli*[3]**
A. Coordination bonds (Å)[1]					
M-$N^{\varepsilon2}_{His56}$	2.20	2.16	2.16	2.19	2.15
M-$N^{\varepsilon2}_{His111}$	2.08	2.23	2.10	2.19	2.06
M-O^{2}_{Asp193}	1.97	1.91	1.98	2.07	1.89
M-$N^{\varepsilon2}_{His197}$	2.20	2.19	2.16	2.21	2.08
M-$O_{coordsolv}$	**2.35**	**2.23**	**2.41**	**2.27**	**1.92**
B. Coordination bond angles (°)					
$N^{\varepsilon2}_{His197}$-M-$N^{\varepsilon2}_{His56}$	93.13	101.54	96.44	89.48	90.66
$N^{\varepsilon2}_{His56}$-M-O^{2}_{Asp193}	84.88	84.95	83.71	83.80	85.66
O^{2}_{Asp193}-M-$O_{coordsolv}$	79.62	83.90	82.11	88.99	91.60
$O_{coordsolv}$-M-$N^{\varepsilon2}_{His111}$	95.70	91.60	89.89	95.74	89.17
$N^{\varepsilon2}_{His111}$-M-$N^{\varepsilon2}_{His197}$	132.42	126.32	131.31	126.68	128.40
C. Hydrogen bonds (Å)					
$O_{coordsolv}$- $O^{\delta1}$ Asp193	2.85	2.95	2.90	2.89	3.03
$N^{\varepsilon1}$Gln178- $O_{coordsolv}$	**2.93**	**2.91**	**2.81**	**2.78**	**3.48**
$N^{\varepsilon1}$Gln178-$O^{\delta1}$ Tyr64	**2.86**	**2.91**	**2.99**	**4.42[4]**	**3.10**
$O^{\delta1}$ Tyr64-O_{water2}	2.75	2.65	2.55	-[4]	2.76
O_{water2}- O_{water3}	2.83	2.74	-	-[4]	3.00
O_{water3}- $N^{\varepsilon1}$His 60	2.90	3.02	5.56	-[4]	2.81

1. The error associated with the bond lengths is ~0.1 Å as calculated from the Cruickshank diffraction-component precision index. 2. The data of Mn-specific SOD was from *H. sapiens* with PDB code: 2P4K, subunit D[36]. 3. Fe-specific SOD was from *E. coli* with PDB code: 1ISB, subunit A[11]. 4. The water mediated hydrogen bond network was interpreted due to the mutation of Tyr64 to Asn64 (named as SOD_{cd}) in PDB 2P4K.

Supporting Figures

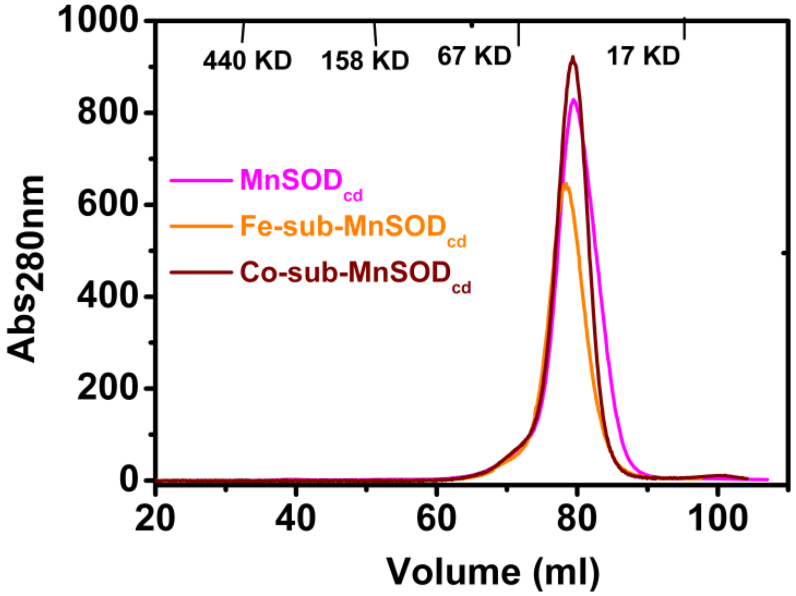

Fig. S1 The superdex 200 gel filtration profiles of different metal ions substituted SODs.

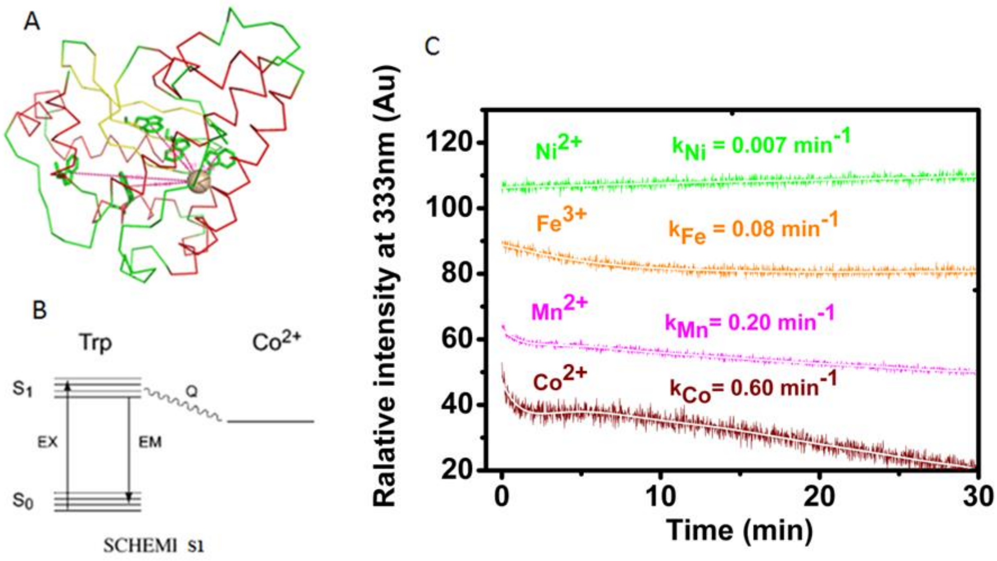

Fig. S2. Intrisinc fluorescence kinetics quenching fro the SOD_{cd} metallation. **Panel A,** the active site of $MnSOD_{cd}$ based on PDB 4JZ2. **Panel B,** schemematically represented the energy transfer between the excited tryptophan residues and the metal center via a Förster transition dipole coupling mechanism[37]. **Panel C,** the metal uptake process of Apo-SOD_{cd} at 40℃ in 20 mM HEPES, pH 7.2, 100 mM NaCl buffer.

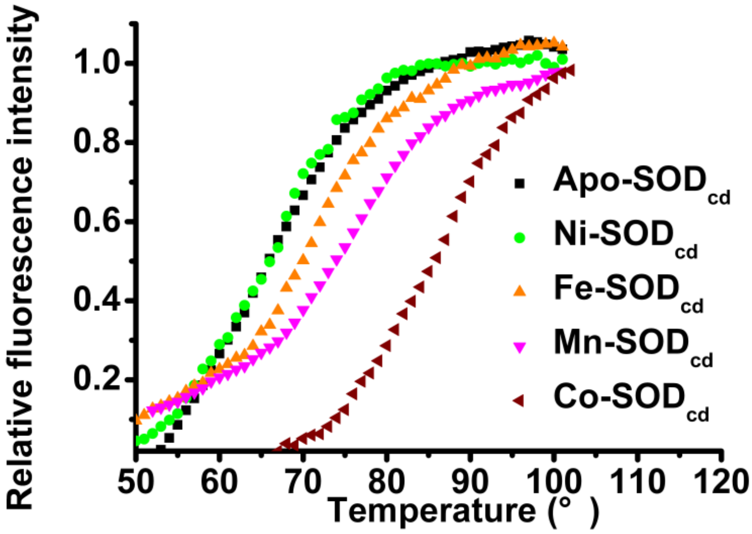

Fig. S3. Thermal denaturation curves for different SOD$_{cd}$s monitored by CD spectroscopy at 222 nm. All the enzyme samples were in 20 mM HEPES, pH 7.2, 100 mM NaCl buffer.

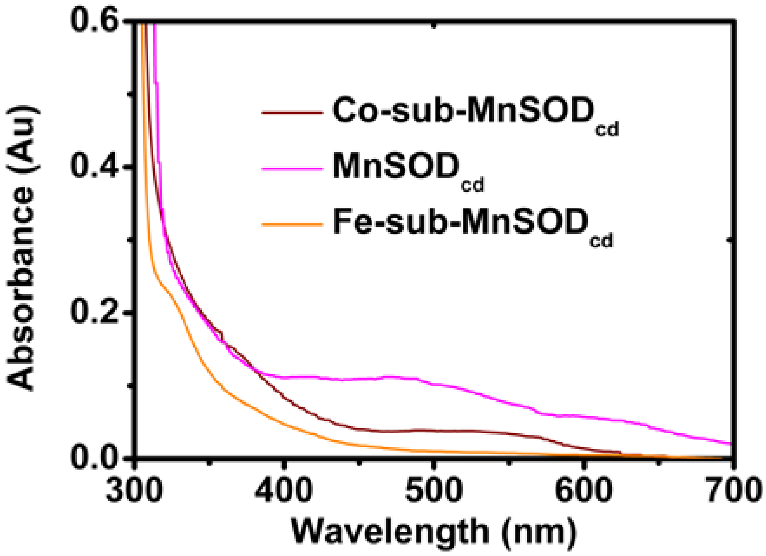

Fig. S4. UV/Vis of SOD_{cd} enzymes. UV/Vis measurements were performed in 100 mM NaCl, 50 mM potassium phosphate, pH 7.4 and the protein concentration was 10 mg/ml.

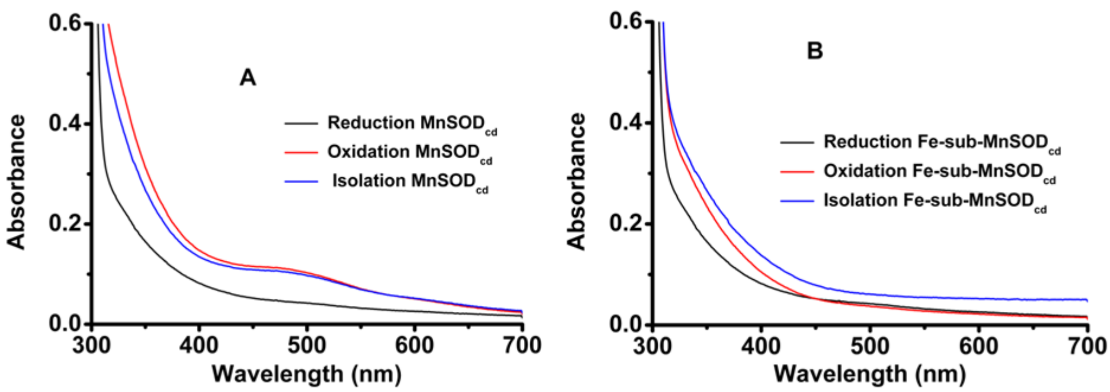

Fig. S5. UV/Vis spectra of $MnSOD_{cd}$ and Fe-sub-$MnSOD_{cd}$. The reduced form was achieved by adding dithionite to the sample and the oxidized form was obtained by addition of substoichiometric $KMnO_4$.

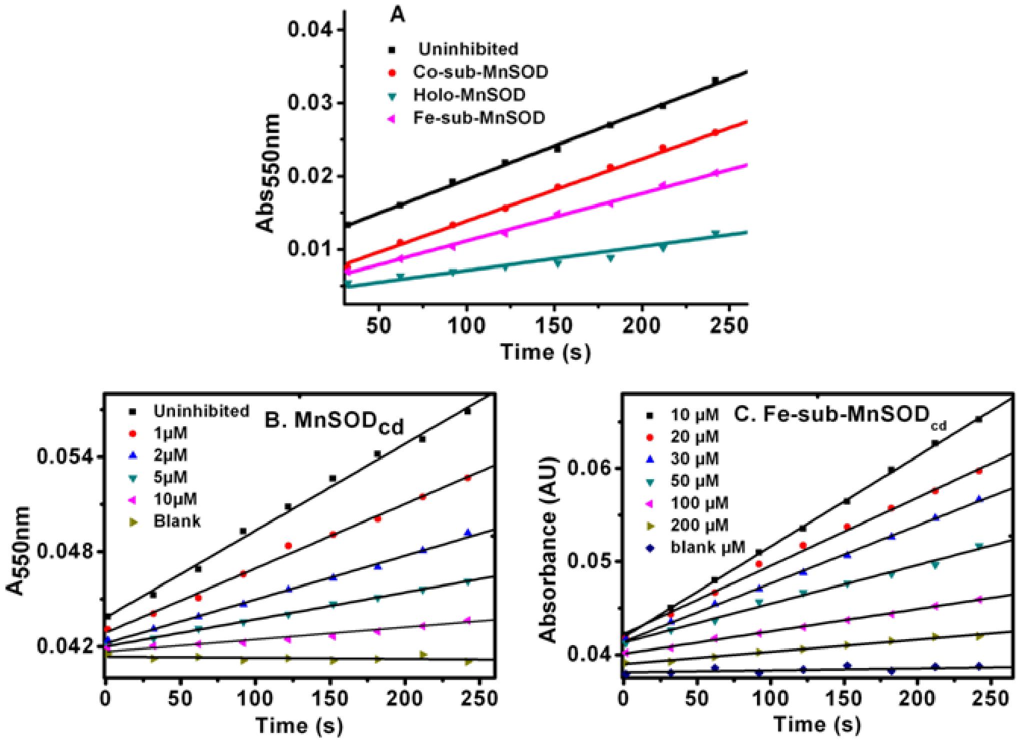

Fig. S6 Xanthine oxidase coupling cyt *c* reduction method for determining the different metal ions substituted SOD_{cd}. Panel A, the ability of SOD_{cd} (3 μM) to inhibit the O_2^- mediated cyt *c* reduction. Panel B and panel C, the concentration dependence of the $MnSOD_{cd}$ and Fe-sub-$MnSOD_{cd}$ activity. The measurement was performed in the standard potassium phosphate buffer at 25℃ and the linear fitting was carried out using Origin 8.0.

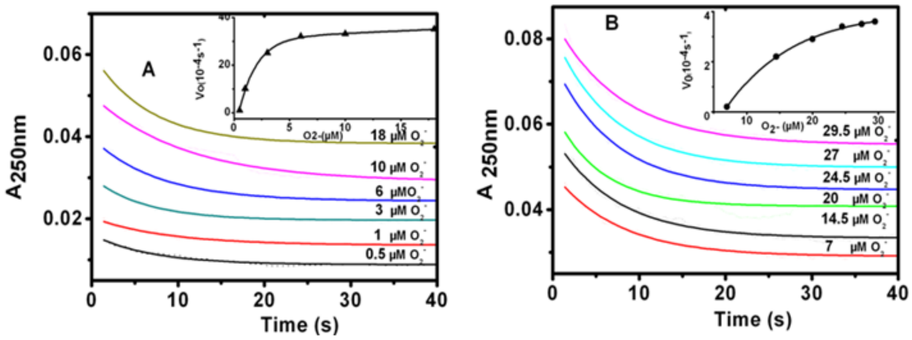

Fig. S7. Stopped-Flow Spectrophotometry for the determination of K_m and k_{cat} values of $MnSOD_{cd}$ and Fe-sub-$MnSOD_{cd}$. Panel A and Panel B are for $MnSOD_{cd}$ and Fe-sub-$MnSOD_{cd}$, respectively.

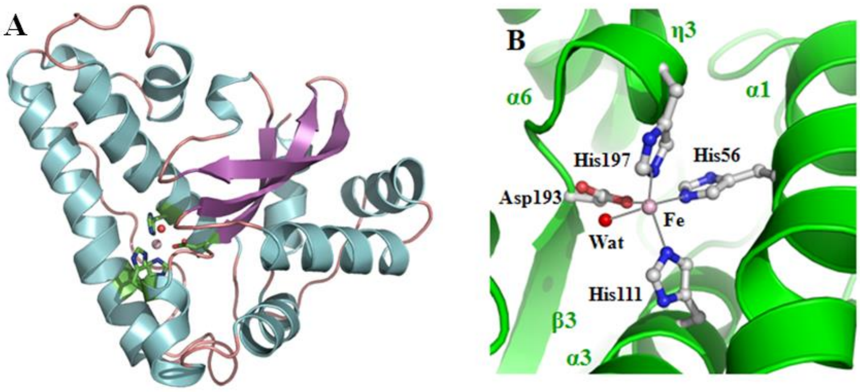

Fig. S8. The overall structure **(A)** and the metal coordinated residues of Fe-sub-MnSOD$_{cd}$ **(B)**.

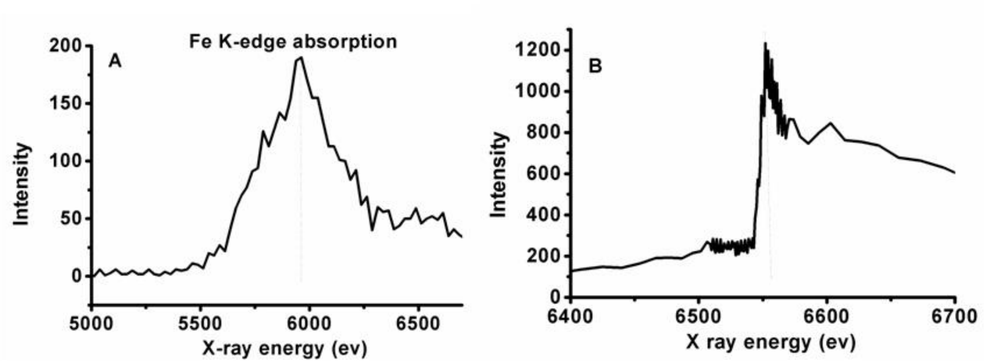

Fig. S9. X-ray absorption specrum **(Panel A)** and X-ray fluorescence spectrum **(Panel B)** of Fe-sub-MnSOD$_{cd}$.

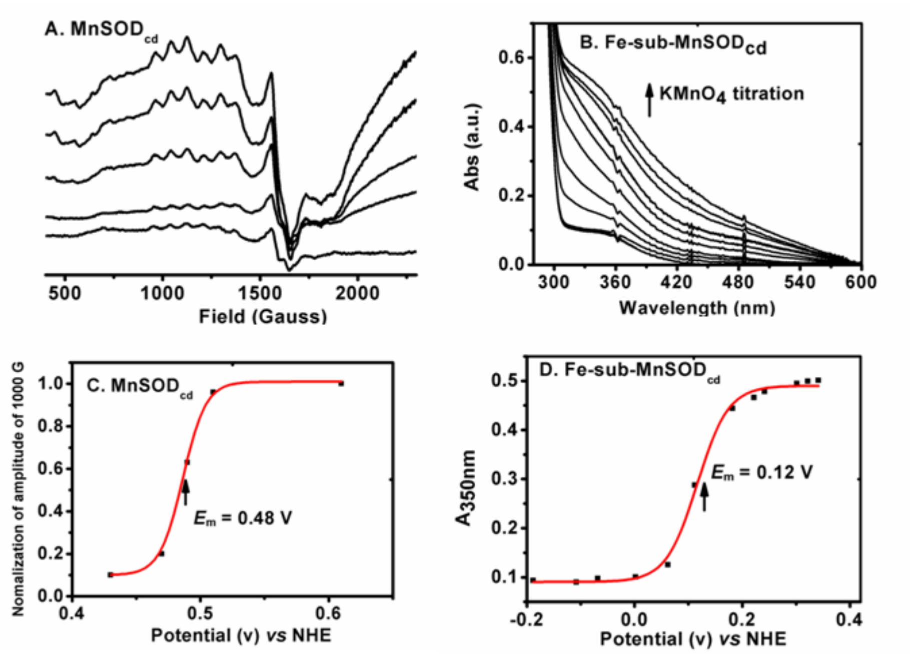

Fig. S10. The potentiometric reductive titration of $MnSOD_{cd}$ *via* EPR spectra (**Panel A, C)** and oxidative titration of Fe-sub-$MnSOD_{cd}$ (**Panel B, D)** by UV/Vis spectra. The quantitative percentage of the oxidative state and reductive state could be inferred by EPR amplitude at g=6.0 for $MnSOD_{cd}$ and the absorption at 350 nm for Fe-sub-$MnSOD_{cd}$ at each equilibrium ambient potential. The Nernst fittings of the [OX]/[RE] as function of ambient potential were shown.

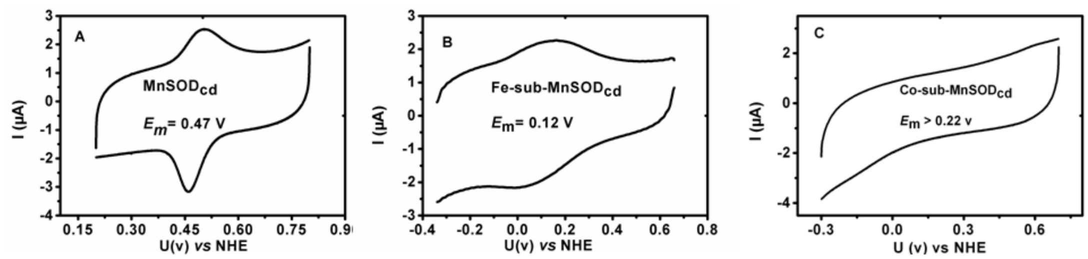

Fig. S11. The CV of $MnSOD_{cd}$ (Panel A), Fe-sub-$MnSOD_{cd}$ (Panel B) and Co-sub-$MnSOD_{cd}$ at NTA-modified glassy carbon electrode in 50 mM PBS buffer (pH 7.4) with a scan rate of 100 mV/S^{-1}.

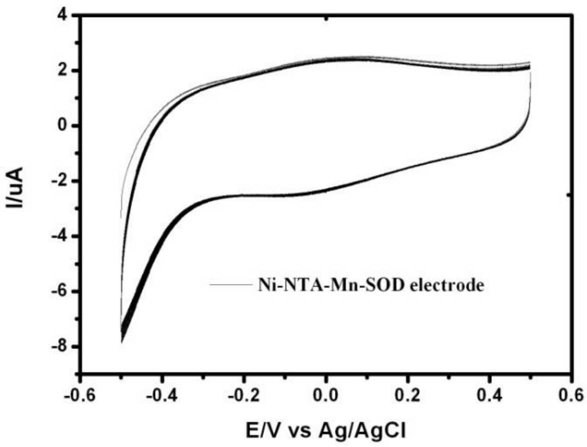

Fig. S12. The numerous time CV scans of Fe-sub-$MnSOD_{cd}$/NTA/GC electrode**.** The scans were performed in 50 mM PBS (pH 7.4) at a rate of 100 mV at the range between -500 mV and +500 mV.

The amperometrical titration of $O_2^{\cdot-}$ for $MnSOD_{cd}$ and Fe-sub-$MnSOD_{cd}$

The direct interaction of $O_2^{\cdot-}$ with the SOD_{cd} modified electrodes were investigated amperometrically at a fixed potential in 50 mM PBS buffer (pH 7.4) under constant stirring on a computer controlled BAS 100 B/W electrochemical analyzer [25] and the CHI604A (Shanghai Chenhua instrument, China). Superoxide was chemically generated in KO_2 + DMSO solution[13]. For the $MnSOD_{cd}$ electrode, the potential was initially held at -400 mV (protein in reduced state) for 10 min reaching to the equilibrium state and we added 50μl (KO_2 + DMSO) solution into the electrolyte when the current-time profile was recorded synchronously and then changed to the second fixed potential of 400 mV (protein in oxidized state), or vice versa. A similar procedure was performed for Fe-sub-$MnSOD_{cd}$ except using potential of -400 mV for the reduced state of the protein and +400 mV for the oxidized state of SOD. The sensitivity of the SOD-based electrodes towards $O_2^{\bullet-}$ is proposed to be dependent on the operation potential and the surface coverage of SOD. As shown in the **Fig. S13,** the $MnSOD_{cd}$ and Fe-sub-$MnSOD_{cd}$/NTA/GC electrodes display amperometric response to successive addition of the KO_2-DMSO solution. Well defined steady-state currents response increasing linearly with $O_2^{\bullet-}$ concentration. Based on the concentration of $O_2^{\bullet-}$ used and the SOD coverage, the sensitivity of $MnSOD_{cd}$ and Fe-sub-$MnSOD_{cd}$ modified electrodes are about 25 and 9 nA cm^{-2}/nM min^{-1}, which are as effective as some reported SOD-based biosensors[38].

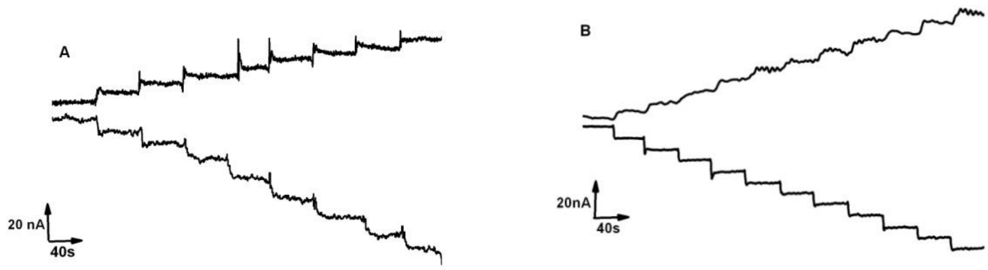

Fig. S13. Typical steady state current-time responses of $MnSOD_{cd}$ and Fe-sub-$MnSOD_{cd}$/NTA/glassy carbon electrode. Panel A is the amperometric response for $MnSOD_{cd}$ at +400 mV for the oxidation of $O_2^{\bullet-}$ and at -400 mV for reduction of $O_2^{\bullet-}$ with every titration of 2μM $O_2^{\bullet-}$. Panel B is amperometric response for Fe-sub-$MnSOD_{cd}$ at +400 mV for the oxidation of $O_2^{\bullet-}$ and at -400 mV for reduction of $O_2^{\bullet-}$ with every titration of 20μM $O_2^{\bullet-}$.

CV behaviors of $MnSOD_{cd}$ and Fe-sub-$MnSOD_{cd}$ at various potential scan rates

In order to assess the adsorption effects of SOD_{cd} on the electrode and the reversibility of the modified SOD electrodes, we performed CV scans at various potential scan rates between 10 mV and 2000 mV for $MnSOD_{cd}$ and 100 mV and 700 mV for Fe-sub-$MnSOD_{cd}$. CVs obtained at the SOD/NTA-modified GC electrodes in phosphate buffer at different potential scan rate clearly show that the peak current (I_p^a and I_p^c) obtained for each SOD are linear with v (but not $v^{1/2}$) in the potential scan range, which reveals that the electron transfer of the SOD_{cd} is a surface-confined process but not a diffusion-controlled one[39]. This is very different from the redox reaction of cyt *c* at the cysteine-modified gold electrode in which the peak current change with $v^{1/2}$, being characteristic of a diffusion-controlled electrode reaction of solution-phase species[40]. The slopes of I_p-v curves are 20.89 for I_p^a and -18.7 for I_p^c of $MnSOD_{cd}$, 17.6 for $I_p^a$and -17.9 for I_p^c of Fe-sub-$MnSOD_{cd}$. The almost comparable slope values suggested a quasi-reversible redox chemistry at the modified electrodes[26]. Interestingly, the current responses of Fe-sub-$MnSOD_{cd}$ along with the various volts, regardless of the anode or cathode, was smaller than that of $MnSOD_{cd}$, which is consistent to the above amperometric titration results of $MnSOD_{cd}$ having more response than Fe-sub-$MnSOD_{cd}$. This justifies the higher activity of $MnSOD_{cd}$ than Fe-sub-$MnSOD_{cd}$.

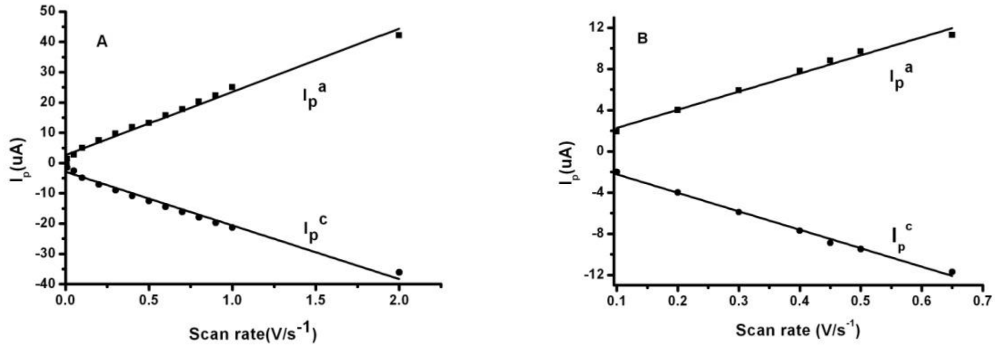

Fig. S14. CV peak current changes as a function of scan rates for MnSOD$_{cd}$ (PanelA) and Fe-sub-MnSOD$_{cd}$ (Panel B). The scan was performed in 50 mM PBS (pH 7.4) at rate range of 0.01-2.0 V/s^{-1} for MnSOD$_{cd}$ and 0.1-0.7 V/s^{-1} for Fe-sub-MnSOD$_{cd}$, respectively. The linear fitting was carried out with Origin 8.0.

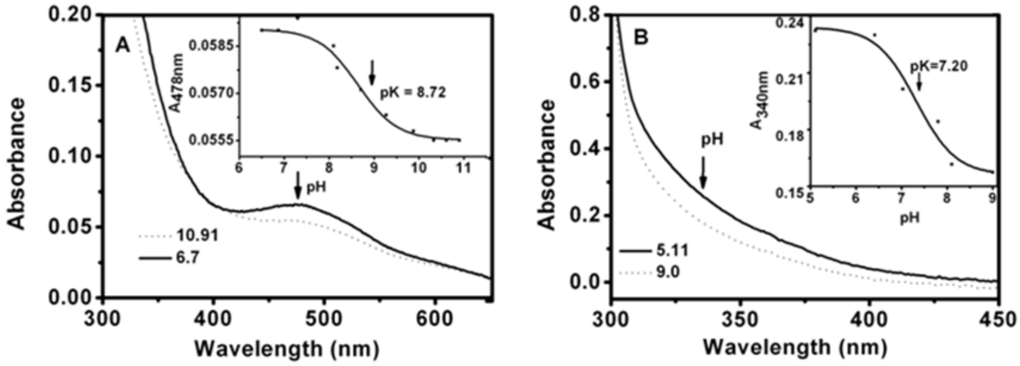

Fig. S15. The optical pH titration of $MnSOD_{cd}$ **(panel A)** and Fe-sub-$MnSOD_{cd}$ **(Panel B)**.

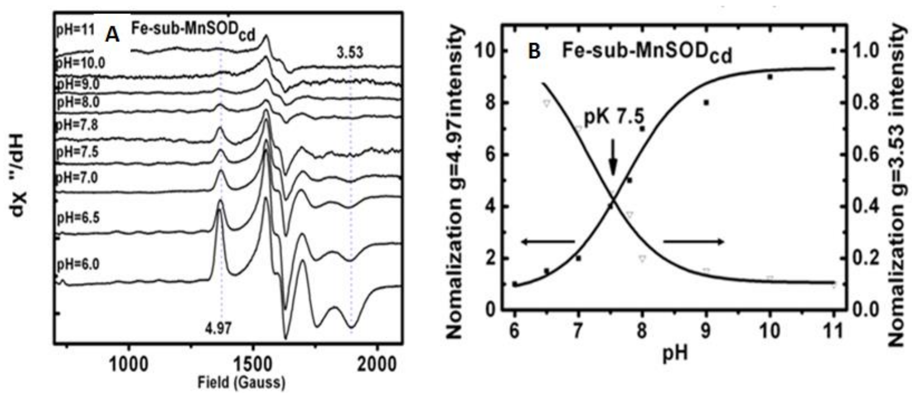

Fig. S16. The relevant EPR signals amplitude change along with pH variation of Fe-sub-$MnSOD_{cd}$. **Panel A,** the different EPR spectra under alterative pH for Fe-sub-$MnSOD_{cd}$. **Panel B,** *pK* values of 7.5 for Fe-sub-$MnSOD_{cd}$ by fitting the signals amplitude change as a function of pH values with Henderson-Hasselbalch (n=1) equation.

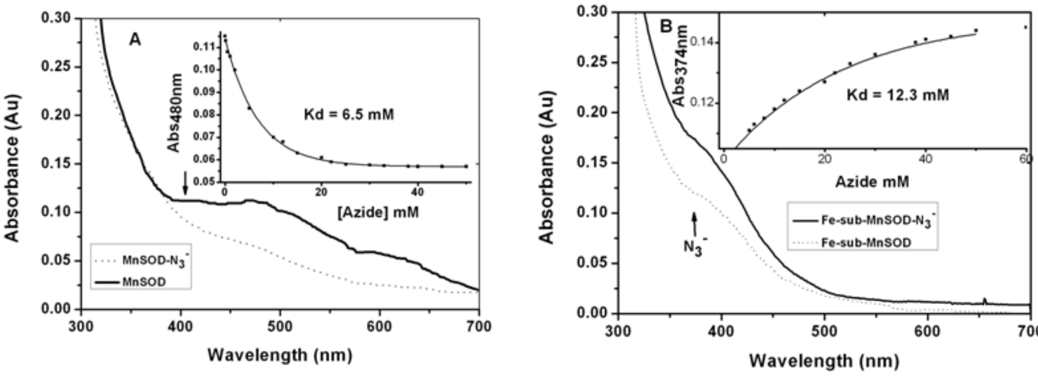

Fig. S17. The optical azide titrations of the two SOD_{cd} enzymes. **Panel A, B** are the spectra of azide binding to $MnSOD_{cd}$ and Fe-sub-SOD_{cd} profiles, respectively. Insets are the fitting curves of the related absorbance change as a function of azide concentration, respectively.

DFT calculation

(1) Computationally-derived Coordinates for $MnSOD_{cd}$, Fe-sub-$MnSOD_{cd}$ and Co-sub-$MnSOD_{cd}$.

Table S4a. Computationally-derived Coordinates for the oxidized $MnSOD_{cd}$

O	0.50531700	1.70858000	0.44391900
C	4.44290100	-5.07717200	-0.11146100
C	5.26245400	-4.01414800	-0.87287500
C	4.50506200	-2.72191400	-0.98742300
C	3.32152900	-2.28336500	-0.43049600
N	5.00356400	-1.61278000	-1.67832400
C	4.15767200	-0.55998600	-1.52229200
N	3.12164800	-0.93346300	-0.75922000
C	-6.58914200	-4.84159300	0.23731100
C	-5.90593400	-3.67137900	-0.52086300
C	-5.33948700	-2.63745300	0.44151900
C	-6.21263800	-1.87585100	1.24017100
C	-3.95925400	-2.43256200	0.60492300
C	-5.73279000	-0.95351900	2.17271800
C	-3.46097800	-1.50911900	1.53190600
C	-4.35251700	-0.77671500	2.31712400
O	-3.81493700	0.16059600	3.22026900
C	-0.76427000	-0.98953100	-5.69878600
C	-0.91015800	-1.99359400	-4.52569800
C	-0.67195000	-1.29404200	-3.22408400
C	0.40827000	-1.31713500	-2.37676600
N	-1.48004900	-0.25634600	-2.74434700
C	-0.89309800	0.31961000	-1.66458800
N	0.26913900	-0.30845300	-1.41140800
C	-5.41820000	4.93973600	-0.19775400
C	-5.81294200	3.45135500	-0.10044500
C	-4.88858600	2.60662800	0.80120000
C	-3.46721100	2.37093000	0.28020900
N	-2.54708600	2.02803900	1.22532500
O	-3.16191600	2.44434600	-0.94262400
C	3.73222800	5.11000900	-2.47011800
C	3.65944800	3.58169700	-2.38467000
C	2.69838000	3.05748900	-1.33570000
O	1.84312000	3.77011300	-0.75555700
O	2.81356000	1.74415400	-1.12197900
C	5.80922400	0.26906900	4.78829900
C	4.52045300	-0.59141000	4.79098200

C	3.52540900	-0.17175500	3.75193600
C	3.40515900	-0.49546400	2.42114600
N	2.50973400	0.76237300	3.98516100
C	1.81958000	0.97774100	2.83299300
N	2.34296000	0.22275700	1.85656900
Mn	1.69963000	0.46605200	-0.12873800
H	6.20566200	-3.81993300	-0.34135400
H	5.54348300	-4.38340500	-1.86847900
H	2.61378000	-2.82049000	0.17550600
H	4.28529400	0.43182100	-1.91690200
H	3.91287000	-4.56932100	0.66697500
H	-6.64721000	-3.18833000	-1.17245600
H	-5.11298300	-4.04930800	-1.17766000
H	-7.28585400	-2.00422700	1.13347000
H	-3.26066400	-3.00837900	0.00434100
H	-6.42868000	-0.37579200	2.77570400
H	-2.39544800	-1.35596200	1.65716100
H	-4.48581300	0.45011500	3.86877000
H	-7.13959300	-4.40722400	1.04605200
H	-0.17401100	-2.79900500	-4.62007400
H	-1.89909400	-2.46941600	-4.55230300
H	1.27008900	-1.95875100	-2.40710700
H	-1.31606100	1.16836500	-1.15145400
H	0.12390200	-0.41096900	-5.55347900
H	-6.83608100	3.35505400	0.28721000
H	-5.81057200	3.01467800	-1.10661900
H	-4.82610900	3.05825000	1.80082000
H	-5.33964000	1.61195000	0.93555600
H	-2.83948800	1.74432500	2.15267700
H	-1.57568000	1.87657700	0.96007200
H	-4.44327100	4.97590800	-0.63804300
H	4.64332800	3.13320000	-2.19914700
H	3.31452200	3.16219500	-3.34217800
H	2.75333300	5.49939000	-2.28269100
H	4.05448900	-0.55923500	5.78439500
H	4.78594900	-1.64030800	4.61566300
H	4.00011800	-1.17695600	1.84137100
H	0.99103000	1.65003900	2.69882000
H	6.48179800	-0.08357300	5.54225200
H	0.75769900	2.62784200	0.13223600
H	5.86345500	-1.59213300	-2.20566700
H	2.31790500	1.20806100	4.86965400
H	-2.36161700	0.05205700	-3.12750000
H	5.06888400	-5.82742500	0.32473800

H	3.72954200	-5.52891400	-0.76880200
H	4.06806800	5.39135200	-3.44637000
H	4.40380200	5.50696000	-1.73768900
H	-0.64398800	-1.47989100	-6.64201400
H	-1.59420700	-0.31382800	-5.69516400
H	5.59303400	1.28514900	5.04489400
H	6.30964300	0.17995000	3.84688900
H	-7.27917200	-5.38110500	-0.37725900
H	-5.85599900	-5.49343300	0.66385800
H	-5.30625200	5.38798100	0.76707400
H	-6.07713100	5.47825300	-0.84630500

Table S4b. Computationally-derived Coordinates for the reduced $MnSOD_{cd}$

O	0.24045400	2.22390700	-0.26041300
C	4.54427900	-5.04870200	1.11593700
C	5.39701000	-4.18520000	0.16223800
C	4.63659500	-2.96282100	-0.26084900
C	3.38638400	-2.49338700	0.08653100
N	5.16677300	-1.97218900	-1.08985600
C	4.25990500	-0.95650400	-1.21061200
N	3.16274900	-1.24052600	-0.50095600
C	-6.49153200	-4.73333300	1.07278400
C	-5.78445400	-3.74350600	0.10221500
C	-5.39307800	-2.47253300	0.84157000
C	-6.39949100	-1.58057600	1.25852500
C	-4.06956000	-2.18941700	1.21715800
C	-6.10533100	-0.46022900	2.03826300
C	-3.75644500	-1.06984900	1.99882200
C	-4.78031100	-0.21829700	2.41493200
O	-4.42589800	0.91364400	3.18197900
C	-0.46950700	-2.35073800	-5.41301900
C	-0.67352400	-3.08832600	-4.06535900
C	-0.61981500	-2.13274000	-2.91577800
C	0.37999900	-1.86911000	-2.01245200
N	-1.58270300	-1.14597200	-2.68004000
C	-1.14963800	-0.32481500	-1.67960600
N	0.05178400	-0.73815700	-1.25146600
C	-5.23605100	4.68551800	-1.56154100
C	-5.60595100	3.25430600	-1.11601900
C	-4.87105600	2.76491000	0.15134900
C	-3.35379800	2.56648500	0.10877800
N	-2.77253900	2.36045100	1.31804000
O	-2.65410100	2.55383200	-0.95238100

C	3.97675300	4.32501500	-3.53845600
C	3.86524000	2.86625400	-3.08533500
C	2.84159600	2.63064900	-1.98781600
O	2.03845500	3.54054200	-1.60710100
O	2.82255300	1.41334300	-1.50105300
C	5.80779300	1.27947900	4.69612500
C	4.48009500	0.48285700	4.81545500
C	3.50904300	0.76789500	3.70269300
C	3.13561000	0.03479400	2.59876400
N	2.79145700	1.96598200	3.58845200
C	2.02922100	1.92631200	2.45555500
N	2.21676800	0.76015400	1.82626500
Mn	1.57984800	0.40107700	-0.23106400
H	6.32129700	-3.87257900	0.66992300
H	5.71211600	-4.77138000	-0.71213400
H	2.63689500	-2.96023000	0.70149700
H	4.39195600	-0.04955300	-1.77309800
H	3.99578300	-4.37522300	1.74086400
H	-6.47119800	-3.49004400	-0.71643500
H	-4.90399700	-4.20811300	-0.35714300
H	-7.43152100	-1.77056700	0.97822100
H	-3.27274500	-2.86285500	0.91491900
H	-6.89928100	0.21340300	2.34960800
H	-2.73710000	-0.86646000	2.30562500
H	-5.17947700	1.24166500	3.70953300
H	-7.06147300	-4.12475800	1.74333200
H	0.11341700	-3.83680800	-3.92331700
H	-1.62448600	-3.63776300	-4.08074200
H	1.31431400	-2.38237200	-1.87652900
H	-1.69939800	0.54013800	-1.34286100
H	0.41860500	-1.75495200	-5.37811200
H	-6.68024900	3.18814200	-0.89726400
H	-5.41221200	2.55702800	-1.94103900
H	-5.08405400	3.45530300	0.97959700
H	-5.29665000	1.79487400	0.44903700
H	-3.31843000	2.14187900	2.14858000
H	-1.76819300	2.24469500	1.35370200
H	-4.24896100	4.61930300	-1.96871500
H	4.82700400	2.46385700	-2.74196400
H	3.55729600	2.22401600	-3.92395400
H	2.99571700	4.74735500	-3.47461900
H	4.00697500	0.69847200	5.78350900
H	4.69025200	-0.59223400	4.81276100
H	3.46749900	-0.94411100	2.30204600

H	1.38741100	2.71971300	2.11276100
H	6.45574600	1.10897300	5.53042100
H	0.86409700	2.89864500	-0.71353300
H	6.07689200	-1.99694500	-1.52354000
H	2.83526300	2.73932000	4.23448400
H	-2.45125900	-1.03639300	-3.18071100
H	5.15192700	-5.67886000	1.73120000
H	3.84691600	-5.63883000	0.55888800
H	4.34269200	4.37426200	-4.54274200
H	4.62980700	4.87906700	-2.89699600
H	-0.32528800	-3.04482200	-6.21449500
H	-1.29402200	-1.69200000	-5.58938800
H	5.59172200	2.32737500	4.70586800
H	6.33450100	0.97620700	3.81551400
H	-7.16692100	-5.39964900	0.57800600
H	-5.77543600	-5.27050600	1.65892800
H	-5.14932000	5.34358300	-0.72215100
H	-5.87265200	5.06139000	-2.33511000
H	-0.68958200	2.35574100	-0.57204600

Table S4c. Computationally-derived Coordinates for the oxidized Fe-sub-MnSOD$_{cd}$

Fe	1.59477200	0.54314000	-0.14760600
O	0.38735900	1.83971600	0.42424900
C	4.42550800	-5.03879800	0.07240400
C	5.26362300	-4.02543600	-0.73629800
C	4.51891100	-2.73711200	-0.91886700
C	3.31451800	-2.29306200	-0.41480600
N	5.03517500	-1.64248100	-1.61726200
C	4.17002100	-0.59302500	-1.51141900
N	3.11221000	-0.95465100	-0.77747100
C	-6.55701200	-4.82247400	0.34843400
C	-5.85768300	-3.68059300	-0.43892200
C	-5.29981100	-2.61763400	0.49665900
C	-6.18097300	-1.82677400	1.25723500
C	-3.92115700	-2.41320500	0.67400500
C	-5.71055200	-0.87803600	2.16776400
C	-3.43228800	-1.46308700	1.57892000
C	-4.33170700	-0.70307700	2.32833100
O	-3.80381200	0.25620500	3.21300600
C	-0.70724700	-1.24295400	-5.63608500
C	-0.86947400	-2.21346600	-4.43583400
C	-0.67956400	-1.45803800	-3.15538200
C	0.38187700	-1.41632100	-2.28660300

N	-1.52121600	-0.41658000	-2.74011500
C	-0.97187200	0.22433700	-1.67804100
N	0.20094500	-0.36567700	-1.37307400
C	-5.34435700	4.94180400	-0.37113900
C	-5.72673700	3.45300300	-0.23913700
C	-4.82768000	2.63993300	0.71276900
C	-3.40094200	2.38410100	0.22220000
N	-2.48923500	2.08169800	1.18441600
O	-3.08732500	2.40820200	-1.00264300
C	3.80874900	5.00989600	-2.55933500
C	3.68051500	3.48823000	-2.43575800
C	2.67801400	3.04767000	-1.38839300
O	1.87550100	3.81717000	-0.81918500
O	2.70957800	1.72159500	-1.15866700
C	5.75923200	0.30483000	4.79119400
C	4.46339400	-0.54425400	4.75087700
C	3.47603900	-0.10801100	3.71053900
C	3.32174400	-0.45845600	2.39033200
N	2.48673300	0.85644800	3.94189700
C	1.77956300	1.06253700	2.79974200
N	2.26580600	0.27257900	1.82897600
H	-6.58800000	-3.21633700	-1.11610600
H	-5.05773000	-4.08350800	-1.07196600
H	-7.25311800	-1.95364100	1.13847300
H	-3.21633700	-3.01084800	0.10266100
H	-6.41263100	-0.27906500	2.74221400
H	-2.36808100	-1.31090300	1.71568700
H	-4.48549900	0.57079000	3.83820100
H	-7.10079900	-4.35869500	1.14464600
H	-6.76108900	3.36425700	0.11959200
H	-5.69188900	2.98641800	-1.23110000
H	-4.78247800	3.12729100	1.69632500
H	-5.28495500	1.65209100	0.87366800
H	-2.79132600	1.84214200	2.12054200
H	-1.50799700	1.93591700	0.93358500
H	-4.36156300	4.99629000	-0.79036400
H	0.59379200	2.76728300	0.13744600
H	3.88289300	-4.49575000	0.81756300
H	6.20531900	-3.81652100	-0.20762700
H	5.54774600	-4.45136500	-1.70825900
H	2.59003200	-2.82380300	0.17714600
H	5.91235000	-1.62751800	-2.11529700
H	4.31114500	0.38462900	-1.93339800
H	0.17100500	-0.65306800	-5.47561200

H	-0.11622600	-3.00713400	-4.47992800
H	-1.84878200	-2.70794100	-4.47159500
H	1.26144100	-2.03296700	-2.27163400
H	-2.40011800	-0.14834600	-3.15795500
H	-1.42571800	1.09295800	-1.21875300
H	2.83712800	5.42814500	-2.39884200
H	4.64158600	3.00789200	-2.21314600
H	3.33848500	3.05028600	-3.38556900
H	6.38868700	-0.04204100	5.58421500
H	3.98424500	-0.52919400	5.73875300
H	4.72566900	-1.59114300	4.56000600
H	3.88694300	-1.16766100	1.81460700
H	2.32213200	1.32521300	4.82005800
H	0.96389800	1.75116900	2.66678500
H	4.18185200	5.26142200	-3.53018200
H	4.47458800	5.40126700	-1.81879100
H	6.30356900	0.20977600	3.87503600
H	5.54862700	1.32693000	5.02708800
H	5.05387300	-5.76912200	0.53763300
H	3.71787000	-5.52407300	-0.56724000
H	-1.54562600	-0.57863700	-5.66157100
H	-0.56744100	-1.74315100	-6.57152400
H	-7.24200800	-5.37803200	-0.25756800
H	-5.83226100	-5.46706600	0.80021200
H	-5.26553400	5.42127200	0.58205700
H	-6.02096600	5.44484000	-1.03036900

Table S4d. Computationally-derived Coordinates for the reduced Fe-sub-MnSOD$_{cd}$

Fe	-1.58470200	-0.38500700	-0.26899400
O	-0.23546700	-2.20782900	-0.16517800
C	-4.46146400	4.99807600	1.06656300
C	-5.33482200	4.14431100	0.12245300
C	-4.60136400	2.91094400	-0.30902500
C	-3.35074600	2.42937100	0.01830300
N	-5.16193300	1.91937500	-1.11440100
C	-4.27030300	0.88859000	-1.23888700
N	-3.15731200	1.16567100	-0.55403700
C	6.52214900	4.72068800	0.94662400
C	5.79581700	3.71893200	0.00310300
C	5.38504200	2.47136200	0.77137500
C	6.37836800	1.58048900	1.22085100
C	4.05449500	2.20707000	1.13586300
C	6.06490500	0.48001900	2.02107300

C	3.72198400	1.10731900	1.93748600
C	4.73321500	0.25688900	2.38567300
O	4.35961100	-0.85404300	3.17362000
C	0.46285800	2.28367100	-5.39320000
C	0.67486600	3.04852700	-4.06007800
C	0.60825400	2.10655500	-2.89699000
C	-0.41309200	1.83151200	-2.02145300
N	1.57764500	1.13335900	-2.62778900
C	1.12731800	0.31029000	-1.63748300
N	-0.09284400	0.70738700	-1.24677700
C	5.21675200	-4.75312200	-1.47501400
C	5.55378500	-3.30215400	-1.06749200
C	4.81511600	-2.79424300	0.19016500
C	3.30071900	-2.58134000	0.13098100
N	2.70972500	-2.33833900	1.32831600
O	2.61198700	-2.58745700	-0.93789200
C	-3.99884800	-4.41396300	-3.34486800
C	-3.85195300	-2.93968800	-2.95706800
C	-2.82262500	-2.67099400	-1.87502900
O	-2.10963500	-3.58883200	-1.36629100
O	-2.71132800	-1.40483700	-1.53613900
C	-5.68496200	-1.10370600	4.78835000
C	-4.35118700	-0.30829300	4.80160700
C	-3.42950700	-0.63359700	3.65574700
C	-3.08780600	0.07221200	2.52439000
N	-2.71453200	-1.83507100	3.54787300
C	-1.98460400	-1.82266900	2.39413400
N	-2.19079500	-0.67166500	1.74196200
H	6.47600200	3.43514800	-0.81124100
H	4.92172100	4.18692300	-0.46501000
H	7.41541200	1.75512200	0.94926500
H	3.26708600	2.87967900	0.80807800
H	6.84930900	-0.19286600	2.35721400
H	2.69702800	0.91846000	2.23464100
H	5.10619400	-1.18043600	3.71204700
H	7.08752200	4.12090800	1.62839100
H	6.62775600	-3.20783800	-0.85768600
H	5.34005800	-2.63131800	-1.90927300
H	5.01540200	-3.47754000	1.02748500
H	5.24712400	-1.82499300	0.48106200
H	3.24997700	-2.10312500	2.15767900
H	1.70525800	-2.21478800	1.34992700
H	4.22211200	-4.73017400	-1.86630900
H	-0.87892100	-2.90598700	-0.53407300

H	-3.89986800	4.33020500	1.68387200
H	-6.25798500	3.84614900	0.64089700
H	-5.65169700	4.73665000	-0.74719300
H	-2.58244600	2.89443200	0.61100100
H	-6.07896900	1.95263700	-1.53238900
H	-4.42570900	-0.01456200	-1.79951900
H	-0.41445400	1.67554900	-5.31271300
H	-0.10647800	3.80517700	-3.93100800
H	1.63050200	3.58903600	-4.08092300
H	-1.35918200	2.32974700	-1.91797100
H	2.46102700	1.03250900	-3.10385600
H	1.67829200	-0.54663200	-1.28376500
H	-3.02647400	-4.85572900	-3.29420000
H	-4.80606800	-2.50567500	-2.62820400
H	-3.53894300	-2.34003100	-3.82382800
H	-6.28711400	-0.90407500	5.65131900
H	-3.82928300	-0.48427900	5.75262300
H	-4.56127800	0.76632200	4.76612900
H	-3.42967800	1.04338300	2.21599100
H	-2.74039900	-2.59408900	4.21158900
H	-1.34516700	-2.61872700	2.05420400
H	-4.40498700	-4.48662800	-4.33314100
H	-4.64521000	-4.93111600	-2.66667200
H	-6.25759000	-0.84448300	3.92305200
H	-5.47483000	-2.15174900	4.83112300
H	-5.06983800	5.63525300	1.67442500
H	-3.77122200	5.59069500	0.50165100
H	1.29482500	1.63310000	-5.56384800
H	0.29690800	2.94376300	-6.21821400
H	7.19190100	5.37547300	0.42835000
H	5.81666200	5.27512300	1.52937200
H	5.16588900	-5.39629200	-0.62182900
H	5.86986600	-5.13078900	-2.23546600
H	0.66701200	-2.34668900	-0.54911400

Table S4e. Computationally-derived Coordinates for the oxidized Co-sub-MnSOD$_{cd}$

C	-3.64429200	5.10206100	-1.01076400
C	-4.51646400	4.04445300	-1.71059800
C	-3.92036400	2.67417000	-1.60694800
C	-2.90007100	2.16401900	-0.83945500
N	-4.42763200	1.57395700	-2.27958600
C	-3.73118100	0.47138200	-1.90388500
N	-2.79495000	0.79726800	-1.02642200

C	7.21827500	4.04910300	0.30698500
C	6.48315300	2.92239100	-0.45401800
C	5.31395200	2.30201600	0.28438300
C	5.50875000	1.28187100	1.22792300
C	3.99408900	2.71216000	0.04005400
C	4.43290000	0.67212200	1.87673200
C	2.90507200	2.10137200	0.66877700
C	3.12391400	1.05977000	1.57270400
O	2.02938900	0.43507800	2.14465200
C	1.53844000	-0.10551300	-5.49041600
C	1.65509900	1.03099000	-4.44347000
C	1.21779400	0.54214200	-3.09591700
C	0.03852400	0.69415500	-2.41304100
N	1.93217500	-0.39282500	-2.35689400
C	1.20110800	-0.77435000	-1.29559200
N	0.03241600	-0.13194400	-1.29442000
C	5.80372200	-4.18246200	1.02861700
C	4.81627800	-3.19025700	1.68609700
C	3.49180300	-2.90703400	0.99555700
N	2.42665200	-2.66813400	1.84771400
O	3.37984600	-2.76956600	-0.22095800
C	-3.66783900	-5.31004100	-1.89072400
C	-3.44594300	-3.80377300	-2.00899000
C	-2.67135200	-3.19605700	-0.85075700
O	-2.12364800	-3.86550100	0.02467100
O	-2.64291500	-1.87608600	-0.90383500
C	-5.76803600	0.63870700	4.41232100
C	-4.42217800	1.39209800	4.43550800
C	-3.36857700	0.90677400	3.47377000
C	-3.40043800	0.36224300	2.21244600
N	-2.01394500	1.05192400	3.75084700
C	-1.28546300	0.60239300	2.70347700
N	-2.10396600	0.18184100	1.74693900
H	-5.51382000	4.02514300	-1.24956100
H	-4.67473300	4.31174500	-2.76345400
H	-2.24460400	2.68400100	-0.15891900
H	-3.91927000	-0.52514800	-2.26839300
H	-3.22563100	4.66763800	-0.12713100
H	7.20517300	2.13511600	-0.70508600
H	6.12360600	3.32282400	-1.40993000
H	3.80812400	3.50929000	-0.67631600
H	6.51891500	0.94937000	1.45577400
H	1.88819400	2.40739900	0.44226700
H	4.60707500	-0.10641700	2.61439800

H	2.23672800	-0.50793600	2.27735300
H	7.65980300	3.67928000	1.20850500
H	1.00599500	1.86702100	-4.72229200
H	2.67671000	1.42832000	-4.40480700
H	-0.80353200	1.32049300	-2.65783200
H	1.54125400	-1.51134300	-0.58833500
H	0.60539100	-0.60009200	-5.31777900
H	6.62131400	-4.18144900	1.71901500
H	5.97446000	-3.95606300	-0.00305100
H	4.63197000	-3.49861600	2.72235800
H	5.30803800	-2.20991000	1.74840900
H	2.45892700	-3.08074700	2.77081700
H	1.49103300	-2.58309200	1.44100700
H	-4.39105000	-3.25680600	-2.11055900
H	-2.86689600	-3.56403100	-2.91203400
H	-2.74616700	-5.76697100	-1.59650800
H	-4.00731800	1.34899100	5.45055700
H	-4.60560500	2.45671700	4.23403600
H	-4.25339200	0.08586000	1.61300900
H	-0.20296400	0.59265600	2.66258800
H	-6.45708800	1.14309800	5.05715400
H	1.50091300	0.26476100	-6.49354800
H	2.31850100	-0.82629300	-5.36049300
H	6.52892100	4.82416700	0.56986900
H	7.98533500	4.44006600	-0.32861700
H	-2.83524100	5.40574900	-1.64177400
H	-4.24538600	5.94169700	-0.73040000
H	-5.67024300	-0.34464400	4.82257500
H	-6.20271100	0.64798700	3.43464000
Co	-1.45799900	-0.68691700	-0.02028900
H	-4.41070400	-5.52066800	-1.14992500
H	-3.99821200	-5.69076400	-2.83454500
O	-0.38577900	-1.91745800	0.86823900
H	-0.91936100	-2.74837100	0.86108500
H	2.86183800	-0.74411100	-2.54870000
H	-1.62630100	1.42643300	4.60643100
H	-5.19815600	1.58462900	-2.93388600
C	5.23953375	-5.61518050	1.05330135
H	4.57741290	-5.75210638	0.22399604
H	6.04466192	-6.31675507	0.98650504
H	4.70452563	-5.77213989	1.96655382

Table S4f. Computationally-derived Coordinates for the reduced Co-sub-MnSOD$_{cd}$

C	-3.95773300	4.94461200	1.88533200
C	-4.88463400	4.32136400	0.82840900
C	-4.25660200	3.11890800	0.19714700
C	-3.06544300	2.47751000	0.43170400
N	-4.88755500	2.33646900	-0.75513500
C	-4.09555200	1.27795000	-1.04839200
N	-2.97828400	1.33081800	-0.33927400
C	6.98561500	3.93427600	1.63631300
C	6.19196000	3.17464200	0.54280300
C	5.61341800	1.87392800	1.07174700
C	6.47397000	0.81474200	1.39903600
C	4.24495300	1.68863400	1.30682900
C	5.99847400	-0.37111400	1.95366900
C	3.74772500	0.50472600	1.85936200
C	4.62946400	-0.52463100	2.19327800
O	4.11055400	-1.67999300	2.74209000
C	0.80059400	2.86913400	-4.97738400
C	1.04819300	3.38534400	-3.54071200
C	0.86632600	2.30317800	-2.52194500
C	-0.21628600	1.97594200	-1.75101000
N	1.77517700	1.28254400	-2.28865500
C	1.23270700	0.39570900	-1.42476800
N	0.01066600	0.78486700	-1.07558000
C	5.68431300	-3.65577400	-1.67764700
C	4.79236800	-3.13238100	-0.52038100
C	3.29765400	-2.87768300	-0.71337800
N	2.56239400	-3.06700800	0.41953900
O	2.77412700	-2.49769100	-1.76753500
C	-4.01632800	-3.68799500	-4.00208800
C	-3.80852800	-2.29993800	-3.40142400
C	-2.83811700	-2.23596700	-2.23279400
O	-2.21776300	-3.24251600	-1.83907100
O	-2.70972400	-1.05125100	-1.73106500
C	-5.53647500	-1.70408700	4.55831300
C	-4.15949100	-1.01649200	4.72601600
C	-3.26417900	-1.16549400	3.52323000
C	-2.96542100	-0.32073300	2.48431900
N	-2.54892300	-2.32133500	3.23455900
C	-1.86755300	-2.14472800	2.07879300
N	-2.09686500	-0.93341600	1.58895800
H	-5.82920600	4.01407500	1.29739300
H	-5.15420000	5.06268300	0.06506700

H	-2.26660700	2.76668000	1.09702800
H	-4.33179400	0.49853600	-1.75455100
H	-3.45508600	4.15492800	2.40364700
H	6.86666300	2.94817700	-0.29247800
H	5.39448000	3.80554100	0.13420700
H	3.54967500	2.49078300	1.07041200
H	7.54179800	0.91849100	1.22313600
H	2.68775400	0.38002700	2.05715200
H	6.69037700	-1.17351400	2.20150700
H	4.83514300	-2.18890200	3.13019900
H	7.51242200	3.19304300	2.20018200
H	0.33561000	4.18193200	-3.30495900
H	2.04648000	3.83273000	-3.46052400
H	-1.14953100	2.50639700	-1.65767800
H	1.74821300	-0.50249100	-1.11956000
H	-0.10954100	2.30682500	-4.99639000
H	6.56365900	-3.95136900	-1.14445500
H	5.75522400	-2.94463100	-2.47397200
H	4.89650800	-3.81679200	0.32919400
H	5.21092600	-2.17506100	-0.17896200
H	3.01600400	-3.05495000	1.32331700
H	1.57760000	-2.82760400	0.38833300
H	-4.75512200	-1.85016700	-3.07636400
H	-3.40510000	-1.60974800	-4.15424100
H	-3.06873300	-4.18298600	-4.04615500
H	-3.64577500	-1.41166100	5.61132500
H	-4.29568000	0.05416300	4.90779200
H	-3.32449500	0.68285800	2.32201100
H	-1.23243400	-2.88866700	1.62340100
H	-6.16351100	-1.61590600	5.42083600
H	0.66634800	3.68086900	-5.66147400
H	1.59284200	2.21782700	-5.28239600
H	6.32075000	4.44479900	2.30130500
H	7.68717300	4.62449800	1.21641500
H	-3.21362300	5.55900400	1.42303200
H	-4.53339500	5.50751600	2.59006500
H	-5.39556600	-2.75594400	4.42175800
H	-6.06196200	-1.23924700	3.75042400
Co	-1.60320100	-0.26818000	-0.32875000
H	-4.68450800	-4.27184100	-3.40412500
H	-4.43294300	-3.57385400	-4.98102300
O	-0.29182900	-2.16433000	-0.52638800
H	0.42499000	-2.16750000	-1.18480800
H	-1.01797300	-2.72508300	-0.96733200

H	2.69144400	1.18761300	-2.70392700
H	-2.53548600	-3.16309300	3.79298400
H	-5.79513000	2.51648700	-1.16041900
C	5.13146686	-4.94336923	-2.31644249
H	4.41712418	-4.68875176	-3.07128318
H	5.93461276	-5.49605524	-2.75734480
H	4.65854344	-5.53992819	-1.56453768

The chemical models of $MnSOD_{cd}$, Fe-sub-$MnSOD_{cd}$ and Co-sub-$MnSOD_{cd}$

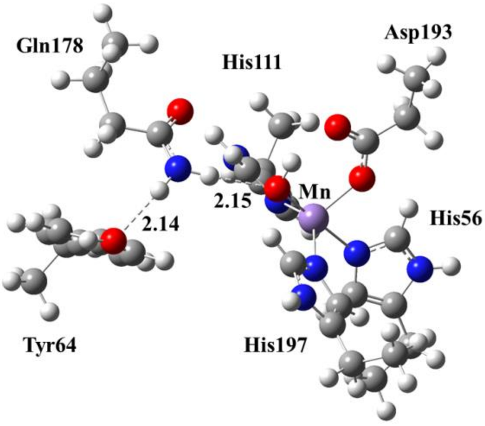

The oxidized MnSOD

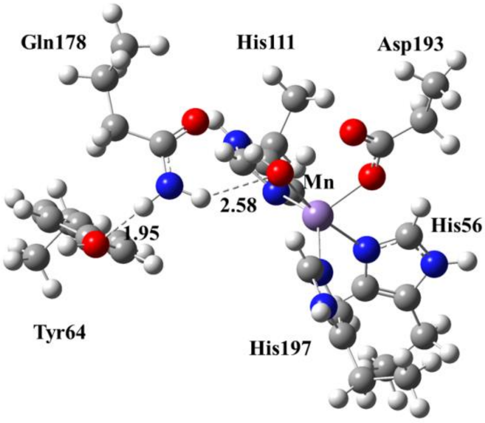

The reduced MnSOD

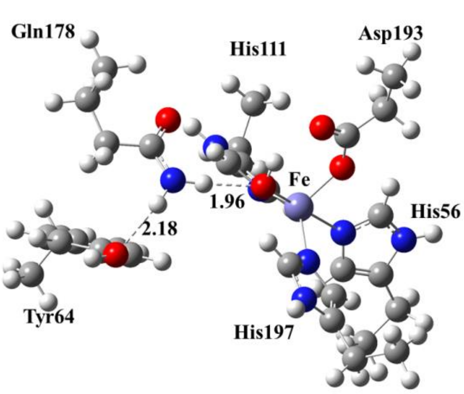

The oxidized FeSOD

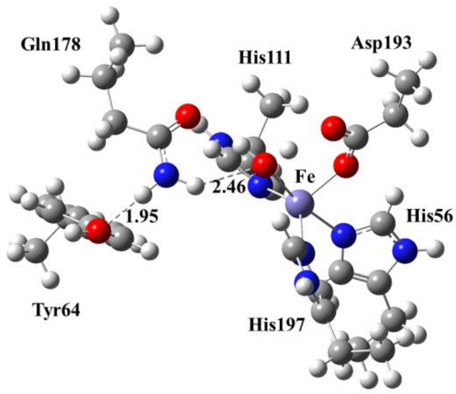

The reduced FeSOD

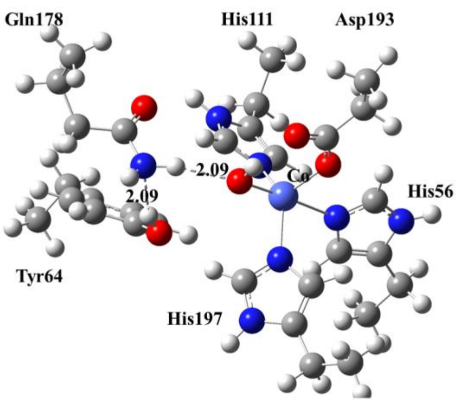

The oxidized CoSOD

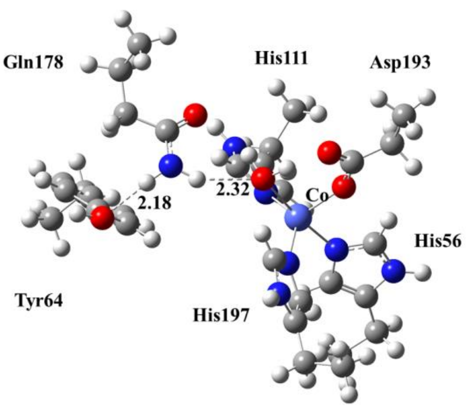

The reduced CoSOD

Fig. S18. The chemical models of $MnSOD_{cd}$, Fe-sub-$MnSOD_{cd}$ and Co-sub-$MnSOD_{cd}$

Table S5. The free energy G at 298K and 101kPa of the reduced $MSOD_{cd}$ (M = Fe^{3+}, Co^{2+}, Mn^{2+}) model and $M(H_2O)_6$ (M = Fe^{3+}, Co^{2+}, Mn^{2+}) are computed at the B3LYP/6-31+g(d,p) -6-31+g(2d,p) level.

	$FeSOD_{cd}$	**$[Fe(H_2O)_6]^{3+}$**	**$CoSOD_{cd}$**	**$[Co(H_2O)_6]^{2+}$**	**$MnSOD_{cd}$**	**$[Mn(H_2O)_6]^{2+}$**
Reduced	-3195.6388	-1721.6998	-3314.9923	-1840.9865	-3083.2855	-1609.3078

Table S6. The reaction free energy ΔG (in kcal/mol) at 298K and 101kPa of substitution reaction.

	$[Fe(H_2O)_6]^{3+}$-sub-$MnSOD_{cd}$	**$[Co(H_2O)_6]^{2+}$-sub-$MnSOD_{cd}$**
ΔG	24.25	-17.69

Table S7. Distance (Å) and E(2) (in kcal/mol) between proton-donor and acceptor atoms of Fe-sub-$MnSOD_{cd,}$ Co-sub-$MnSOD_{cd}$ and $MnSOD_{cd}$.

Reactant	**Gln178-N-H…O-H**		**Gln178-N-H…O-Tyr64**	
	distance	**E(2)**	**distance**	**E(2)**
Oxidized FeSOD	1.96	4.36	2.18	2.77
Reduced FeSOD	2.46	0.74	1.95	5.87
Oxidized MnSOD	2.15	2.62	2.14	3.10
Reduced MnSOD	2.58	0.43	1.95	5.97

References

1. X. Zhu, X. Gu, S. Zhang, Y. Liu, Z. X. Huang and X. Tan, *Protein Expr Purif*, 2011, **78**, 86-93.
2. F. Yamakura, K. Kobayashi, H. Ue and M. Konno, *European Journal of Biochemistry*, 1995, **227**, 700-706.
3. M. M. Bradford, *Anal Biochem*, 1976, **72**, 248-254.
4. R. S. Hall, D. F. Xiang, C. Xu and F. M. Raushel, *Biochemistry*, 2007, **46**, 7942-7952.
5. M. M. Whittaker, K. Mizuno, H. P. B ähinger and J. W. Whittaker, *Biophysical Journal*, 2006, **90**, 598-607.
6. Y. P. Lin, C. J. Kuo, X. Koleci, S. P. McDonough and Y. F. Chang, *J Biol Chem*, 2011, **286**, 3957-3969.
7. G. W. T. M.J. Frisch, H.B. Schlegel, G.E. Scuseria, M.A. Robb, J.R. Cheesman, J.A. Montgomery, Jr., T. Vreven, K.N. Kudin, J.C. Burant, J.M. Millam, S.S. Iyengar, J. Tomasi, V.Barone, B. Mennucci, M. Cossi, G. Scalmani, G.A. Petersson, H. Nakatsuji, M. Hada, M. Ehara, K. Toyota, R. Fukuda, J. Hasegawa, M. Ishoda, T. Nakajima, Y. Honda, O. Kitao, H. Nakai, M. Klene, X. Li, J.E. Knox, H.P. Hratchian, J.B.Cross, C. Adamo, J. Jaramillo, R. Gomperts, R.E. Stratmann, O. Yazyev, A.J. Austin, R. Cammi, C.Pomelli, J. Otcherski, P.Y. Ayala, K. Morokuma, G.A. Voth, P.Salvador, J.J. Danneberg, V.G. Zakrzewski, S. Dapprich, A.D. Daniels, M.C. Strain, O. Farkas, D.K. Malick, A.D. Rabuck, K. Raghavachari, J.B. Foresman, J.V. Ortiz, Q. Cui, A. Baboul, S. Clifford, J. and B. B. S. Cioslowski, G. Liu, A. Liashenko, P. Piskorz, I. Kamaromi, L.R. Martin, D.J. Fox, T. Keith, M.A. Al- Laham, C.Y. Peng, A. Nanaykkara, M. Challacombe, P.M.W. Gill, B. Johnson, W. Chen, M.W. Wong, G. Gonzalez, J.A. Pople, *Gaussian Inc.*, 2003.
8. M. Ando, Y. C. Manabe, P. J. Converse, E. Miyazaki, R. Harrison, J. R. Murphy and W. R. Bishai, *Infect Immun*, 2003, **71**, 2584-2590.
9. M. Osawa, F. Yamakura, M. Mihara, Y. Okubo, K. Yamada and B. Y. Hiraoka, *Biochim Biophys Acta*, 2010, **9**, 6.
10. J. M. McCord and I. Fridovich, *J Biol Chem*, 1969, **244**, 6049-6055.
11. M. S. Lah, M. M. Dixon, K. A. Pattridge, W. C. Stallings, J. A. Fee and M. L. Ludwig, *Biochemistry*, 1995, **34**, 1646-1660.
12. G. J. McClune and J. A. Fee, *Biophys J*, 1978, **24**, 65-69.
13. S. Marklund, *J Biol Chem*, 1976, **251**, 7504-7507.
14. Z. Otwinowski and W. Minor, in *Methods in Enzymology*, ed. Charles W. Carter, Jr., Academic Press, 1997, pp. 307-326.
15. A. Vagin and A. Teplyakov, *Journal of Applied Crystallography*, 1997, **30**, 1022-1025.
16. P. Liu, H. E. Ewis, Y. J. Huang, C. D. Lu, P. C. Tai and I. T. Weber, *Acta Crystallogr Sect F Struct Biol Cryst Commun*, 2007, **63**, 1003-1007.
17. G. N. Murshudov, A. A. Vagin and E. J. Dodson, *Acta Crystallogr D Biol Crystallogr*, 1997, **53**, 240-255.
18. P. Emsley and K. Cowtan, *Acta Crystallogr D Biol Crystallogr*, 2004, **60**, 2126-2132.
19. P. D. Adams, P. V. Afonine, G. Bunkoczi, V. B. Chen, I. W. Davis, N. Echols, J. J. Headd, L. W. Hung, G. J. Kapral, R. W. Grosse-Kunstleve, A. J. McCoy, N. W. Moriarty, R. Oeffner, R.

J. Read, D. C. Richardson, J. S. Richardson, T. C. Terwilliger and P. H. Zwart, *Acta Crystallogr D Biol Crystallogr*, 2010, **66**, 213-221.

20. R. A. Laskowski, M. W. MacArthur, D. S. Moss and J. M. Thornton, *Journal of Applied Crystallography*, 1993, **26**, 283-291.
21. M. Pasi, M. Tiberti, A. Arrigoni and E. Papaleo, *J Chem Inf Model*, 2012, **5**, 5.
22. M. A. Walsh, G. Evans, R. Sanishvili, I. Dementieva and A. Joachimiak, *Acta Crystallographica Section D*, 1999, **55**, 1726-1732.
23. M. T. Stankovich, *Anal Biochem*, 1980, **109**, 295-308.
24. V. J. Leveque, C. K. Vance, H. S. Nick and D. N. Silverman, *Biochemistry*, 2001, **40**, 10586-10591.
25. N. B. Surmeli, N. K. Litterman, A.-F. Miller and J. T. Groves, *Journal of the American Chemical Society*, **132**, 17174-17185.
26. K. B. Oldham and C. G. Zoski, in *Comprehensive Chemical Kinetics*, eds. C. H. Bamford and R. G. Compton, Elsevier, 1986, pp. 79-143.
27. B. M. E. Cances, J. Tomasi, *J. Chem. Phys.*, 1997, **107**, 3032-3041.
28. V. B. M. Cossi, B Mennucci, J. Tomasi, *ChemPhysLett*, 1998, **286**, 253-260.
29. A. D. Becke, *Phys Rev A*, 1988, **38**, 3098-3100.
30. A. D. Becke, *J. Chem. Phys.*, 1993, **98**, 1372 - 1377.
31. A. D. Becke, *J. Chem. Phys.*, 1993, **98**, 5648 - 5652.
32. J. Almlöf, Taylor, PR., *Adv Quant Chem*, 1991, **22**, 301.
33. C. Geslin, J. Llanos, D. Prieur and C. Jeanthon, *Res Microbiol*, 2001, **152**, 901-905.
34. E. D. Glendening, C. R. Landis and F. Weinhold, *Wiley Interdisciplinary Reviews: Computational Molecular Science*, 2012, **2**, 1-42.
35. D. W. Cruickshank, *Acta Crystallogr D Biol Crystallogr*, 1999, **55**, 583-601.
36. J. J. Perry, A. S. Hearn, D. E. Cabelli, H. S. Nick, J. A. Tainer and D. N. Silverman, *Biochemistry*, 2009, **48**, 3417-3424.
37. M. M. Whittaker and J. W. Whittaker, *Biochemistry*, 2008, **47**, 11625-11636.
38. B. Prieto-Simón, M. Cortina, M. Campàs and C. Calas-Blanchard, *Sensors and Actuators B: Chemical*, 2008, **129**, 459-466.
39. Y. Tian, L. Mao, T. Okajima and T. Ohsaka, *Anal Chem*, 2004, **76**, 4162-4168.
40. Y. L. Sun, Y. H. Wang, M. M. Yan, B. Y. Sun, Y. Xie, Z. X. Huang, S. K. Jiang and H. M. Wu, *J Mol Biol*, 1999, **285**, 347-359.